Geomorphology 386 (2021) 107746

Contents lists available at ScienceDirect

Geomorphology

journal homepage: www.elsevier.com/locate/geomorph

Sinkhole development in the Sivas gypsum karst, Turkey

Ergin Gökkaya [a,*], Francisco Gutiérrez [b], Mateja Ferk [c], Tolga Görüm [d]

[a] Department of Geography, Ankara University, Turkey
[b] Department of Earth Sciences, University of Zaragoza, Spain
[c] Anton Melik Geographical Institute, Research Centre of the Slovenian Academy of Sciences and Arts, Slovenia
[d] Eurasia Institute of Earth Sciences, Istanbul Technical University, Turkey

ARTICLE INFO

Article history:
Received 14 February 2021
Received in revised form 10 April 2021
Accepted 12 April 2021
Available online 14 April 2021

Keywords:
Evaporite karst
Collapse
Solutional denudation
Morphometry
Sinkhole hazard

ABSTRACT

The extensive gypsum karst of Sivas, Turkey is one of the most outstanding examples of bare gypsum karst in the world. It displays a number of remarkable geomorphic features, including: (1) two stepped planation surfaces cut-across folded gypsum developed during an initial phase of slow base level deepening punctuated by periods of stability; (2) unusual deeply entrenched gypsum canyons related to a subsequent phase of rapid fluvial incision and water table lowering; (3) a polygonal karst of superlative quality mainly developed in the upper surface; (4) relict valleys disrupted by sinkholes in the lower erosional surface; (5) a large number of bedrock collapse sinkholes mostly associated with the lower surface; and (6) numerous cover subsidence sinkholes developed in the valley floors. This work analyses the spatial distribution, characteristics and evolution of the sinkholes within the broad Plio-Quaternary geomorphological and paleohydrological evolution of the epigene karst system dominated by autogenic recharge. A cartographic sinkhole inventory has been produced in an area covering 2820 km^2 with morphometric data and including 295 bedrock collapse sinkholes and 302 cover subsidence sinkholes. The different sinkhole types show a general spatial zonation controlled by the hydrogeological functioning of the different sectors: (1) solution sinkholes (polygonal karst) in the upper recharge area; (2) bedrock collapse sinkholes in the lower denudation surface and close to the base level, where well developed caves are inferred; and (3) cover subsidence sinkholes, with high densities probably associated with areas of preferred groundwater discharge. The morphology of the bedrock collapse sinkholes, varying from small cylindrical holes to large and deep tronco-conical depressions with gentle slopes reflect to geomorphic evolution of these sinkholes that reach exceptionally large hectometre-scale diameters. Their evolution, involving substantial enlargement and deepening, is attributed to the solutional removal as solute load of large volumes of gypsum by downward vadose flow. This type of morphological evolution with significant post-collapse solutional denudation differs from that observed in carbonate rocks characterised by lower solubility and erodibility. The analysis of historical imagery reveals that bedrock collapse sinkholes currently have a very low probability of occurrence and that buried cover subsidence sinkholes are used for urban development creating risk situations.

© 2021 The Author(s). Published by Elsevier B.V. This is an open access article under the CC BY license (http://creativecommons.org/licenses/by/4.0/).

1. Introduction

Gypsum karst has received limited attention compared with limestone karst, despite its widespread worldwide distribution and the higher speed of the associated dissolution and ground deformation processes, potentially leading to severe engineering and environmental problems (Klimchouk et al., 1996b; Cooper and Gutiérrez, 2013). It is estimated that around 25% of the continental surface is underlain by evaporitic formations, which commonly include significant Ca-sulphate units (gypsum and/or anhydrite; Ford and Williams, 2007). Gypsum karst displays similar geomorphic features to those found in carbonate karst terrains, but has a number of distinctive characteristics mainly related to the rate of morphogenetic processes, the development time and size of the resulting landforms, as well as their preservation potential (Cooper, 1998; Paukštys et al., 1999; Cooper et al., 2011): (1) Gypsum has significantly higher solubility than carbonate rocks (2.6 g L^{-1}), its dissolution is not affected by sources of acidity (e.g. carbon dioxide, sulphuric acid), and dissolves much faster. Consequently, surface and subsurface solutional landforms form and evolve more rapidly and cave systems can adjust promptly to changes in base level. (2) Gypsum formations, due to their high solubility and mechanical erodibility, are less suitable to form extensive outcrops with bare karst terrain and rarely occur forming prominent reliefs, unless there are favourable conditions (e.g. arid climate, uplift, differential erosion). (3) Gypsum rock has lower mechanical strength than carbonate formations. Moreover,

* Corresponding author at: Department of Geography, Ankara University, Sıhhiye, 06100 Ankara, Turkey.
E-mail addresses: egokkaya@ankara.edu.tr (E. Gökkaya), fgutier@unizar.es (F. Gutiérrez), mateja.ferk@zrc-sazu.si (M. Ferk), tgorum@itu.edu.tr (T. Görüm).

https://doi.org/10.1016/j.geomorph.2021.107746
0169-555X/© 2021 The Author(s). Published by Elsevier B.V. This is an open access article under the CC BY license (http://creativecommons.org/licenses/by/4.0/).

rapid dissolution acting along discontinuity planes (i.e. fractures, bedding planes) can significantly reduce its rock mass strength over short time spans. Relevant implications of this feature include that underground cavities display smaller spans, bedrock collapse sinkholes at the time of formation reach lower dimensions and caves have lower preservation potential. (4) Gypsum has a more ductile rheology than carbonate rocks. This explains why sagging is a relatively common subsidence mechanism in evaporite terrains (e.g. Guerrero et al., 2008). (5) Subsurface dissolution of gypsum (interstratal karst, mantled karst) through the migration of dissolution fronts can result in the development of widespread subsidence phenomena, generating large-scale gravitational deformation structures and extensive dissolution-induced basins (Gutiérrez and Cooper, 2013 and references therein). (6) The various types of subsidence sinkholes, which are the main geohazard endemic to karst areas, typically show a much higher probability of occurrence due to the faster rate of dissolution and deformation processes (Gutiérrez, 2016). (7) The mitigation of geotechnical problems related to gypsum dissolution commonly require immediate action in order to arrest the quick growth of cavities through positive feed-back mechanisms (e.g., leakage in dams; Gutiérrez et al., 2015).

A significant proportion of the gypsum karst investigations have been focused on the characterisation of cave systems developed in epigene and hypogene hydrogeological systems (Calaforra and Pulido-Bosch, 2003; Stafford et al., 2008; Klimchouk, 2013; De Waele et al., 2017) and on the analysis of hazardous sinkhole areas (e.g., Cooper, 1998; Galve et al., 2009; Fidelibus et al., 2011). Nonetheless, there are few comprehensive geomorphological investigations carried out in bare gypsum karst areas, probably due to the scarcity of this type of karst settings and the greater attention received by carbonate outcrops.

The Central Anatolian Plateau in Turkey includes outstanding outcrops of Cenozoic gypsum formations (Fig. 1). Neogene gypsum formations deposited in several lacustrine basins form extensive exposures around Ankara. In these areas, gypsum karst landscapes are not well developed, but gypsum karst problems have resulted in significant economic losses (e.g. Gökkaya and Tunçel, 2019). In contrast, the vast exposure of Paleogene gypsum deposited in shallow marine and sabkha environments of the Sivas Basin displays karst landforms of superlative quality (Waltham, 2002) and constitutes one of the most remarkable bare gypsum karst landscapes in the world (Fig. 1). It displays exceptional landforms and landscapes due to their rarity, dimensions and abundance: (1) denudation surfaces with magnificent polygonal karst landscape, rarely observed in gypsum terrains; (2) uncommon long and deeply entrenched gypsum canyons; (3) high numbers bedrock collapse sinkholes that reach exceptional dimensions; (4) other depressions rarely documented in gypsum karst terrains, such as relict valleys and poljes. Evaporite karst areas, despite their potential outstanding value, have been barely considered from the geoheritage perspective. Williams (2011) reviewed the numerous natural properties of the UNESCO World Heritage List with internationally significant karst features and analysed the representation of the various types of karst. He identified the following significant gaps in the existing coverage: (1) evaporite karsts are not represented; (2) lack of karst landscapes associated with arid and semiarid environments; and (3) numerous remarkable karst landscapes in the Middle East and Central Asia do not feature on the list. The incorporation of the Sivas gypsum karst, with outstanding universal value, could contribute to fill those significant gaps of the World Heritage List.

The Sivas gypsum karst has been described in several publications (Alagöz, 1967; Waltham, 2002; Doğan and Yeşilyurt, 2004; Doğan and Özel, 2005; Doğan and Yeşilyurt, 2019). Doğan and Özel (2005) studied the central sector of the vast gypsum karst area differentiating two main phases of karst development (i.e., young and mature). Other specific studies deal with hydrogeology (Kaçaroğlu et al., 1997; Günay, 2002), sinkhole susceptibility (Yılmaz, 2007), density of sinkholes (Poyraz

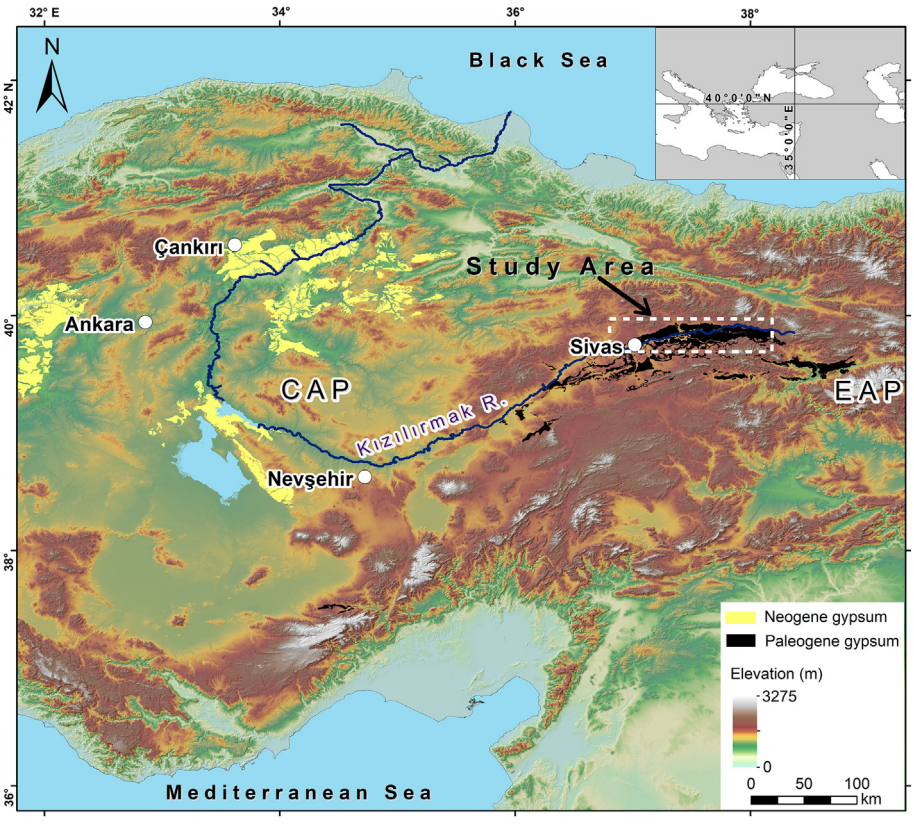

Fig. 1. Geographic location of the Sivas gypsum karst (black polygons) within the Anatolian Platform, traversed by the partially allogenic Kızılırmak River. Yellow polygons indicate the distribution of Neogene gypsum in Turkey. Distribution of evaporite outcrops derived from MTA (2002). CAP: Central Anatolian Plateau; EAP: Eastern Anatolian Plateau.

et al., 2021), geoheritage (Akbulut, 2011; Yılmaz, 2012) and geophysical site investigations (Drahor, 2019; Özel and Darıcı, 2020). This work reconstructs the geomorphological and paleohydrological evolution of the Sivas gypsum karst and analyses the development of various types of sinkholes on the basis of a comprehensive cartographic inventory covering 2820 km^2. Special attention is paid to the numerous bedrock collapse sinkholes, which reach exceptionally large densities and dimensions.

2. Regional setting

The Sivas gypsum karst is located at the transition zone between the Central Anatolian Plateau and the Eastern Anatolian Plateau (Fig. 1). The area has a continental climate with a mean annual temperature of around 9 °C and 436 mm in average annual precipitation, with most of the rain falling during spring. The gypsum karst terrain mainly occurs in the northern sector of the E-W-oriented Sivas Basin, which is around 200 km long and 50 km wide. This foreland basin is situated at the junction between three crustal blocks: the Kırşehir metamorphic massif on its western border, the Pontides thrust belt to the north, and the Tauride–Anatolide continental block to the south (Yılmaz and Yılmaz, 2006). The development of the basin started after the closure of the Northern Tethys Ocean during the Upper Cretaceous, accompanied by the southward obduction of ophiolitic blocks onto the carbonate platform (Guezou et al., 1996; Poisson et al., 1996, 2016). The sedimentary fill of the Sivas Basin comprises several stratigraphic series that record the different phases of its paleogeographic evolution, in chronological order: (1) Eocene turbidites (flysch) of the Bozbel Fm. (Kurtman, 1973) accumulated in relation with the Tauride collision (Callot et al., 2014). (2) Evaporites of the Hafik (or Tuzhisar) Fm. deposited in an environment evolving progressively from shallow marine to sabkha under arid to semi-arid climate during the Late Eocene (Kurtman, 1973; Gündoğan et al., 2005; Legeay et al., 2019). This evaporite formation, up to around 1000 m thick, dominantly crops out on the northern sector of the basin, which corresponds to the karst area investigated in this work. It is mainly composed of Ca-sulphates (gypsum and anhydrite) and includes halite units in the subsurface, as revealed by halokinetic structures to the south, saline springs and the Celalli-1 hydrocarbon-exploration well, south of the study area, which penetrated 89 m of pure salt at a depth of 2111 m below the ground surface (Onal et al., 2008) (Fig. 2B). South of the investigated sector salt tectonics has produced different generations of salt walls and minibasins (i.e. salt-withdrawal basins; Callot et al., 2014; Kergaravat et al., 2017). However, it is not known whether the Hafik Fm. includes significant salt units in the study area. (3) The dominantly red fluvial clastics of the Lower Oligocene Selimiye Fm. record the first continental sedimentation following regional emergence. (4) The Late Oligocene fluvio-lacustrine red beds of the Karayün Fm. were deposited in the central and southern part of the basin (Kurtman, 1973; Gündoğan et al., 2005; Ribes et al., 2018). (5) Early Miocene shallow marine limestones, sandstones and marls of the Karacaören Fm. deposited as a result of renewed marine transgression in the central and eastern part of the basin (Kurtman, 1973; Akkiraz et al., 2018; Ribes et al., 2018). (6) Middle Miocene to Early Pliocene fluvial conglomerate, sandstone and mudstone of the Benlikaya Fm., mostly exposed south of the evaporite domain (Poisson et al., 1996; Ribes et al., 2015). (7) Fluvial conglomerates, sandstones and lacustrine marls and limestones of the Incesu Fm., Late Miocene to Early Pliocene in age according to vertebrate fauna (Poisson et al., 1996). Outcrops of this formation mainly occur in the northern and western part of the evaporite domain area. (8) Late Pliocene lacustrine limestones and sandstones of the Meraküm Fm. that form the caprock of a plateau northwest of Sivas (Fig. 2). (9) Quaternary travertine and alluvial deposits.

The main compressional deformation phase that affected the basin sediments occurred during the Miocene, in relation with the continental collision between the Arabian and Eurasian Plates (Cater et al., 1991; Poisson et al., 1992; Guezou et al., 1996). The NNW-SSE-oriented contraction caused the development of double-verging thrusts faults directed to the north and south (Poisson et al., 1992). The folds and thrusts display a prevalent WSW-ENE to E-W trend. In the neotectonic period (Late Miocene to present) two different thrust systems developed in the study area. One of these corresponds to S-verging E-W faults, located south of the study area. (Yılmaz and Yılmaz, 2006; Poisson et al., 2016). The other one is the WSW-ENE to E-W striking Sivas Thrust, which has transported the evaporites of the Hafik Fm. to the north (Fig. 2B).

The main structures present in the study area are genetically related to the N-verging Sivas Thrust (Poisson et al., 2016). This thrust system overrides the Late Miocene-Early Pliocene Incesu Formation (Temiz, 1996; Poisson et al., 2016) (Fig. 2B). It also deforms the Late Pliocene Meraküm Formation as well as Quaternary deposits (Poisson et al., 1996). Therefore, the thrust can be considered as an active Quaternary structure (Poisson et al., 1992, 1996). Yılmaz and Yılmaz (2006) stated that the sediments of the Sivas Basin experienced significant deformation during the Quaternary period. Hot springs along the Sivas Thrust and Quaternary travertines found in these areas (Fig. 2B) also support the Quaternary activity of the thrust.

3. Materials and methods

The Sivas gypsum karst was analysed using geological and geomorphological data. We produced a geomorphological map and a sinkhole cartographic inventory using the following sources of data: (1) a digital surface model and derived relief models with a horizontal resolution of 5 m (Turkish General Directorate of Mapping); (2) multi-temporal satellite images available in Google Earth; (3) multiple sets of aerial photographs (1966, 1973, 2015) printed at an approximate scale of 1:40,000; and (4) topographic maps with contour intervals of 10 m. The mapped area reaches 110 km in length in the E-W direction, is around 20 km wide and covers approximately 2820 km^2 (Fig. 2). We used the Red Relief Image Map (RRIM) visualization method with the digital surface model data to map sinkholes and other geomorphic features. The main concept of the RRIM method, as proposed by Chiba et al. (2008), is combining three topographic element layers: slope, positive openness, and negative openness (Fig. 3). Positive openness and negative openness layers (Yokoyama et al., 2002) were produced with SAGA GIS. Negative openness has higher values in valleys and in the inner part of karst depressions, while positive openness has higher values on the margins of karst depressions and ridges. Both are combined in the so-called Ridge and Valley Index (I):

$$I = (Op - On)/2$$

where Op is positive openness, and On is negative openness. The RRIM map combines two images: (1) the *I* index which emphasizes convex and concave landforms with a grey gradation; and (2) the topographic slope represented with chroma values of red, which is the richest tone for human eyes. The resulting RRIM model eliminates the dependency of shaded relief images on incident light direction and emphasizes topographic convexity and concavity at the same time (Chiba et al., 2008). RRIM facilitates the identification of karst depressions by shading the side slopes and lightening the divides of the enclosed basins in a polygonal karst (Fig. 3). The morphometric characteristics were measured using GIS software (i.e. ArcMap). Subsequently, we conducted a thorough field survey to confirm the mapped sinkholes and other geomorphic features, as well as to refine the final map.

4. Results

4.1. Main geomorphological features and long-term landscape evolution

The youngest marine sediments deposited in the area are the Early Miocene limestones of the Karacaören Fm., which occur as fragmentary inliers within the vast outcrop of the Late Eocene Hafik Fm. These

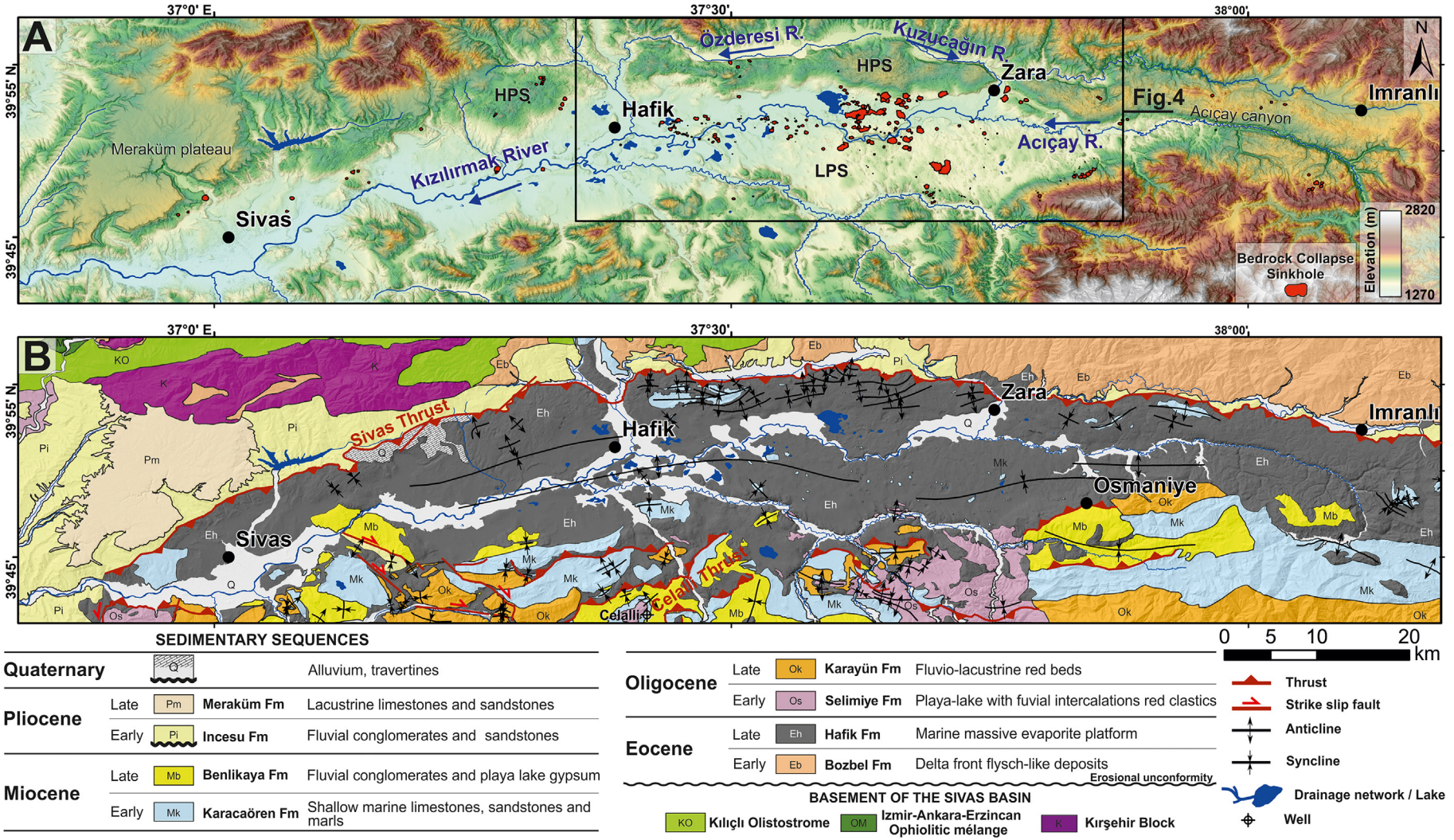

Fig. 2. General geomorphic and geological configuration of the analysed area in the Sivas gypsum karst. (A) Relief model showing the main geomorphic features and the distribution of the bedrock collapse sinkholes. HPS: High Plateau Surface. LPS: Low Plateau Surface (Base map: TanDEM-X data). (B) Geological sketch of the investigated area. Grey area indicates gypsum outcrops, bounded to the north by the Sivas Thrust and to the south by a complex suite of salt walls and salt-withdrawal basins. Adapted from Kurtman (1973) and Legeay et al. (2019).

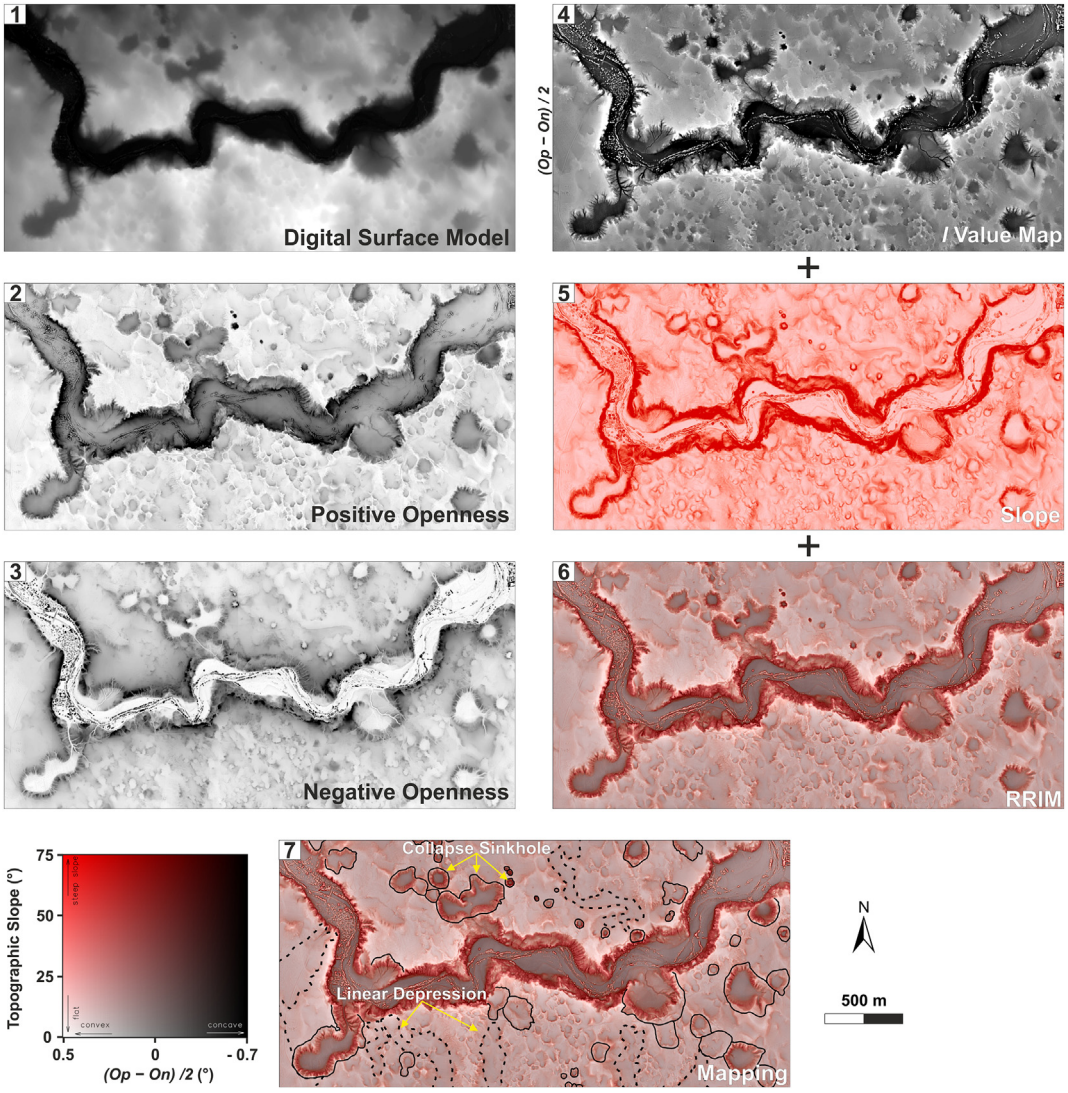

Fig. 3. Images showing different topographic data layers derived from the digital surface model used for the generation of the Red Relief Image Map (RRIM), which facilitates the identification of sinkholes and the delineation of their edges. Sample area of the Low Plateau Surface entrenched by the Tödürge Canyon. Solid polygons indicate bedrock collapse sinkholes and dashed lines relict valleys. Solution sinkholes forming a polygonal karst are not delineated. See explanation in the text.

sediments reveal that the investigated zone was largely submerged by the sea during the Early Miocene marine transgression. The initiation of the long-term erosion processes that led to the progressive erosional removal of the formations overlying the gypsum can be situated sometime after the deposition of the Early Miocene limestones of the Karacaören Fm.. The exposure of the gypsum to the action of rain, runoff and direct infiltration water allowed the development of the bare gypsum karst landscape of Sivas.

Two plateau-like erosional surfaces of different ages and cut-across folded gypsum can be differentiated (Alagöz, 1967; Doğan and Özel, 2005) (Figs. 4, 5). The oldest and highest surface, traditionally designated as the High Plateau Surface (HPS), occurs as a long E-W-oriented and 115 km long strip located north of the Kızılırmak River, in the upthrown block of the Sivas Thrust. This erosional surface lies at 1500–1620 m a.s.l. and truncates folded Late Eocene gypsum (Hafik Fm.) and locally Early Miocene limestones (Karacaören Fm.). West of Sivas city, in the footwall of the Sivas Thrust, there is an extensive outcrop of Late Pliocene lacustrine limestones (Meraküm Fm.), which forms a large structural platform known as the Meraküm Plateau (Fig. 2). This plateau, with a general NW tilt away from the Sivas Thrust, reaches an elevation of around 1650 m a.s.l. The fact that this plateau (footwall of Sivas Thrust) is situated at a higher elevation than the HPS (hanging wall of Sivas Thrust) indicates that the HPS is inset into the Meraküm Plateau and has a younger age (Late Pliocene-Quaternary). The Kızılırmak River is deeply entrenched into the Meraküm Plateau as much as 400 m. Considering 3.6 Ma as the age of the base of the Late Pliocene, a minimum long-term incision rate of 0.11 mm/yr can be estimated for this fluvial system. The actual rate could be significantly higher, since the incision of the Kızılırmak River probably started in the Quaternary; then the maximum age could be 2.6 Ma and the minimum incision rate would be 0.15 mm/yr. Numerical dating of the surfaces and deposits that bracket the onset of fluvial incision would allow to obtain more precise downcutting rates. The gypsum in the HPS is pockmarked by densely packed solution sinkholes forming a striking polygonal karst landscape (Fig. 5).

The youngest planation surface, inset into the HPS, is the Low Plateau Surface (LPS), dissected by the Kızılırmak River (Figs. 4, 5). This erosional plateau, lying between 1320 and 1485 m a.s.l. and perched 30–135 m above the river, can be ascribed to the Quaternary. The LPS displays a different karst landscape than the HPS, with relict valleys and a large number of bedrock collapse sinkholes (Figs. 4, 5). The overall lowering of the base level recorded by the different perched geomorphic surfaces on both the footwall and hanging-wall of the Sivas Thrust is the response to regional uplift within a compressional tectonic

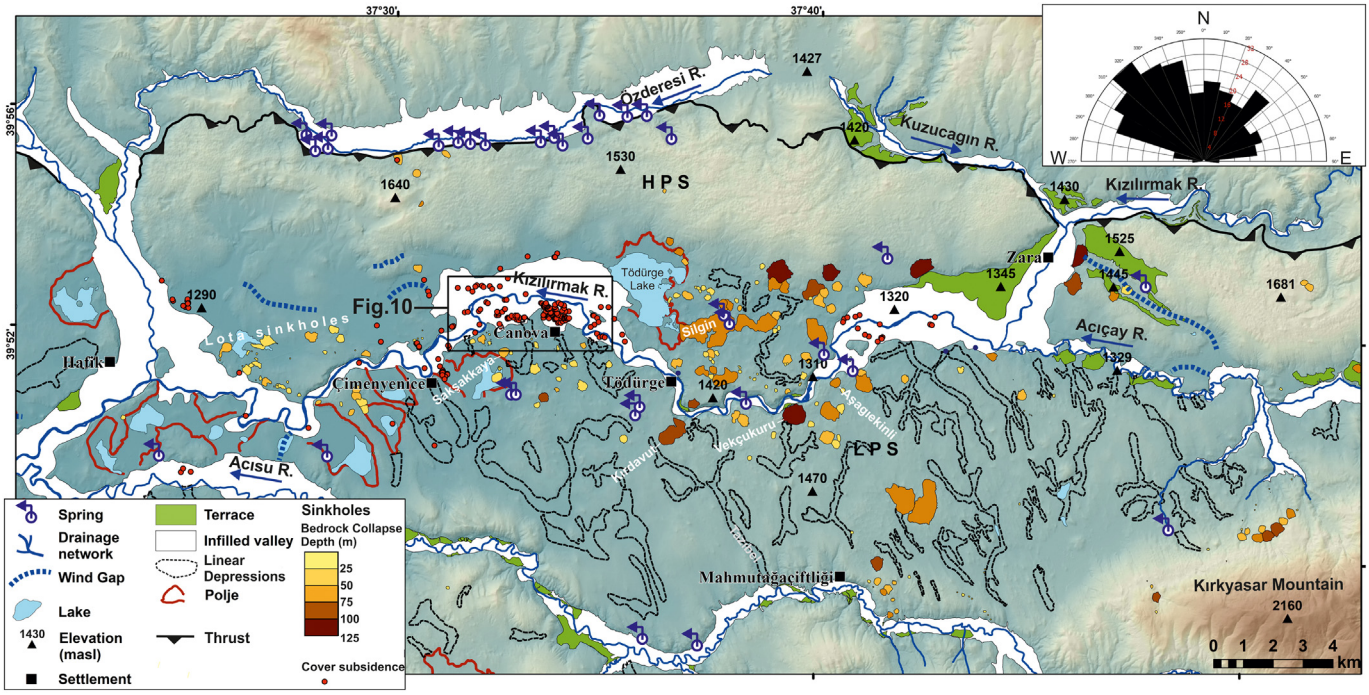

Fig. 4. Geomorphological map of the central sector of the study area where bedrock collapse sinkholes display the highest density. Bedrock collapse sinkholes classified according to their depth. Inset rose diagram depicts the frequency of the orientation of the major axis of bedrock collapse sinkholes, both single and compound.

environment that occurred during the late Cenozoic. At the present time, the Early Miocene marine sediments of the Karacaören Fm. are situated at 1400–1600 m a.s.l. in the central sector, while they reach 1800–2000 m a.s.l. in the eastern sector, recording substantial late Cenozoic differential uplift with an E-W gradient.

The drainage network has a dominant W-E orientation parallel to the structural grain and apparently controlled by active tectonic structures (Fig. 2). The N-verging Sivas Thrust, which is expressed in the landscape as a prominent and poorly dissected gypsum escarpment with rectilinear segments, controls the path of several drainages, from east to west: Kızılırmak (upstream of Zara), Kuzucagın and Özderesi rivers. These longitudinal streams largely flow along asymmetric valleys carved next to the leading edge of the Sivas Thrust on its footwall. In the vicinity of Zara and Hafik, the rivers show sharp bends and flow to the south, traversing perpendicularly the Sivas Thrust and flowing along water gaps carved into the gypsum that underlies the High Plateau Surface (Figs. 2A, 4). The regional base level of the Sivas gypsum karst is controlled by the Acıçay and the Kızılırmak rivers, which define an E-W trending drainage line probably controlled by differential tectonic subsidence south of the Sivas Thrust (e.g. trailing syncline related to a thrust ramp). Regional uplift and the associated fluvial entrenchment have resulted in the development of striking gypsum canyons, which are geomorphic features relatively uncommon in evaporites compared with the less erodible and mechanically stronger carbonate rocks. The Acıçay Canyon, located east of the study area is one of the longest (24 km) and deepest (275 m) canyons in Central Anatolia. The floor of the canyon ranges from 1530 to 1400 m. The name of the canyon refers to the bitter taste of the water, fed by many calcium-sulphate-rich karst springs. West of the canyon and south of Zara, the Acıçay River joins the Kızılırmak River. The 130 m deep and 9.2 km long Tödürge Canyon, carved into LPS by the Kızılırmak River is located east of the Tödürge Lake (Figs. 4, 5). South of the study area, the Acısu River (meaning bitter water) has incised a canyon 215 m deep and 30 km long.

East of Zara there is a SE-NW oriented abandoned valley that connects the Acıçay and the Kızılırmak valleys (Fig. 4). This 5 km long and around 830 m wide wind gap is inset 170 m into the High Plateau Surface and is perched some 94–100 m above the bottom of the Acıçay and the Kızılırmak valleys. Its NW gradient indicates that it corresponds to a former valley section of the Acıçay River, which was abandoned when the headward propagation of a tributary of the Kızılırmak, associated to an elbow south of Zara, captured the Acıçay River (Fig. 4). The northern margin of the wind gap shows disconnected fluvial terraces that record the southward migration of the river when it was located in this position. Both the distribution of terraces and the capture-related diversion of the Acıçay River to the south are consistent with differential vertical tectonic movements, including uplift in the HPS associated with the Sivas Thrust and relative subsidence along the drainage line defined by the Acıçay and Kızılırmak rivers. The bottom of the perched paleovalley shows a large sinkhole 410 m across, formed after the abandonment of the valley section and most probably related to the progressive drop of the base level by fluvial entrenchment.

4.2. Sinkholes

A cartographic sinkhole inventory of the study area has been constructed in a GIS environment, including a total of 295 bedrock collapse sinkholes and 302 cover subsidence sinkholes. The latter can be related to collapse, sagging and/or suffosion (Gutiérrez et al., 2008), but the available information restricted to surface observations does not allow an unambiguous classification of these sinkholes. At least 19 sinkholes with scarped edges are of the cover-collapse type, but diffuse-edged cover sinkholes could also correspond to collapse sinkholes with degraded margins, as well as to suffosion and sagging sinkholes. The thousands of solution sinkholes that occur on the extensive gypsum outcrops forming a polygonal karst landscape, mainly in the High Plateau Surface (Fig. 5), are not addressed in this work (Waltham, 2002; Doğan and Özel, 2005; Doğan and Yeşilyurt, 2019; Poyraz et al., 2021). The inventory includes qualitative and quantitative information for each sinkhole that was used for the analysis of their morphometric characteristics, spatial distribution, controlling factors, and morphological evolution. The qualitative data include: (1) sinkhole typology, referring to the material affected by settlement and the inferred subsidence mechanisms; (2) geomorphic position; (3) single versus compound depression; (4) closed versus open by the external drainage network;

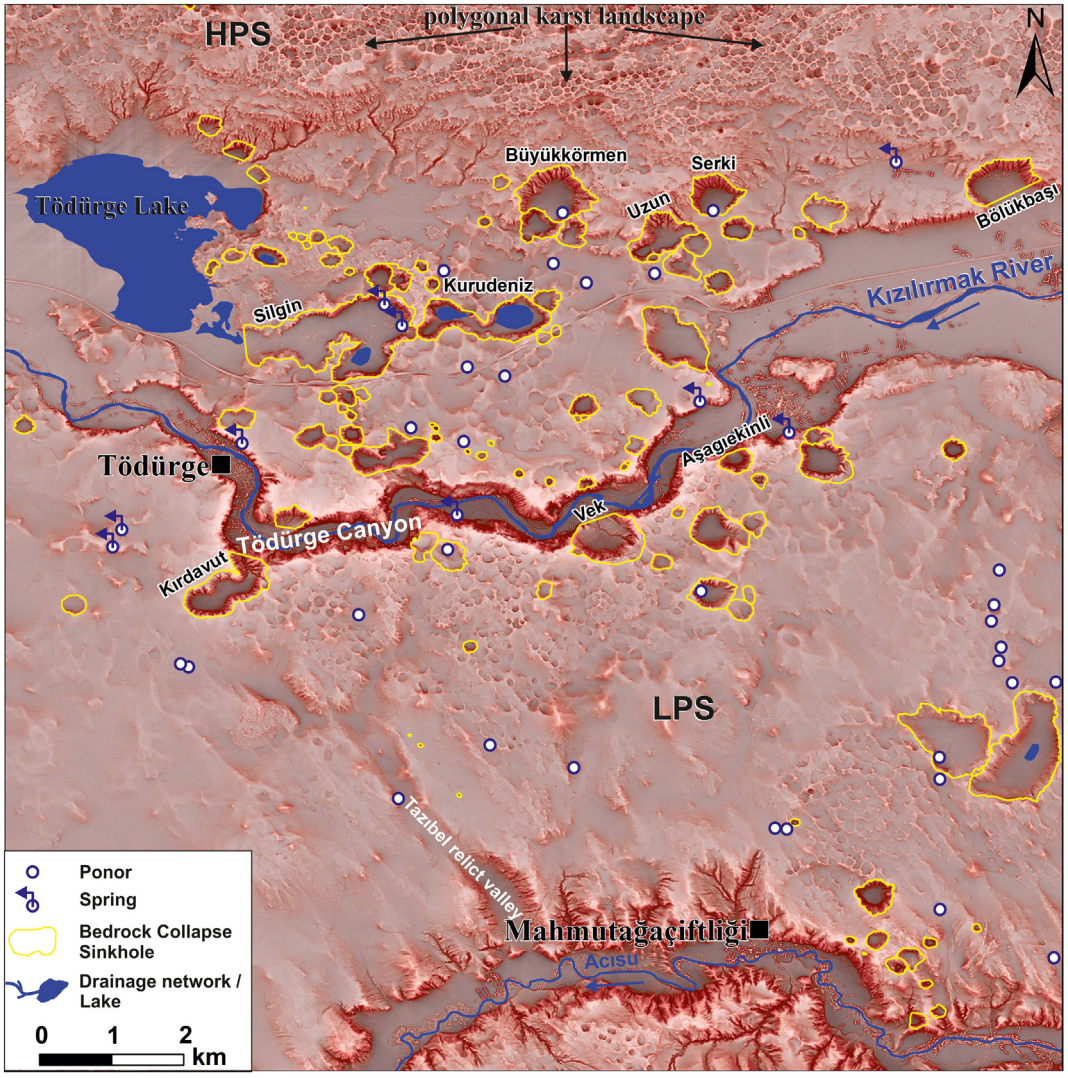

Fig. 5. Red Relief Image Model of the central sector of the study area illustrating the distribution of single and compound bedrock collapse sinkholes. Note the striking polygonal karst landscape developed in the High Plateau Surface (HPS).

(5) with or without lake; (6) presence of mass movements at the margins; (7) relative chronology based on their degree of degradation (e.g. cylindrical versus tronco-conical). The numerical data cover the following features (e.g. Gutiérrez et al., 2019; Parenti et al., 2020): (1) geographical coordinates of the centroid; (2) major axis; (3) orientation of major axis; (4) elongation ratio, given by the relation between the diameter of a circle with the same area as that of the depression and the major axis of the sinkhole; (5) area; (6) perimeter; (7) circularity ratio, defined as the ratio between the area of the depression and the area of a circle having a circumference equal to the perimeter of the depression; (8) depth, given by the maximum vertical distance between the sinkhole edge and its bottom; (9) volume, estimated from the area of the depression and the average depth; (10) elevation of sinkhole floor. The major axis, area and volume of the sinkholes were used to analyse their size distribution and generate empirical frequency-size relationships.

4.2.1. Bedrock collapse sinkholes

A total of 295 bedrock collapse sinkholes have been mapped with an aggregate area of 17.1 km^2. These values, together with the area of the minimum bounding polygon that encloses all the bedrock collapse sinkholes (1072.4 km^2), yield sinkhole densities by number and percentage area of 0.28 sinkholes/km^2 and 1.6%, respectively. A number of these depressions host permanent or ephemeral lakes and others display

Table 1
Main morphometric parameters of the single and compound bedrock collapse sinkholes extracted from the cartographic inventory.

Parameter	Single sinkholes				Compound sinkholes			
	Maximum	Minimum	Average	Standard deviation	Maximum	Minimum	Average	Standard deviation
Major axis (m)	904.87	8.84	211.82	170.72	1911.85	82.25	530.30	426.11
Circularity ratio	0.98	0.59	0.86	0.09	0.93	0.32	0.66	0.15
Elongation ratio	0.96	0.63	0.85	0.06	0.87	0.55	0.74	0.08
Area (m^2)	428,295.98	41.55	39,972.128	60,934.76	1,341,632.78	3298.36	176,052.29	273,420.65
Perimeter (m)	2938.80	24.18	613.93	509.75	7297.20	237.00	1582.26	1419.51
Volume (m^3)	12,582,185.69	2.87	620,511.42	1,572,946.46	28,325,361.52	3543.30	3,212,843.08	6,076,763.02
Depth (m)	125.46	0.01	26.19	25.83	98,25	3,05	36,00	23,40

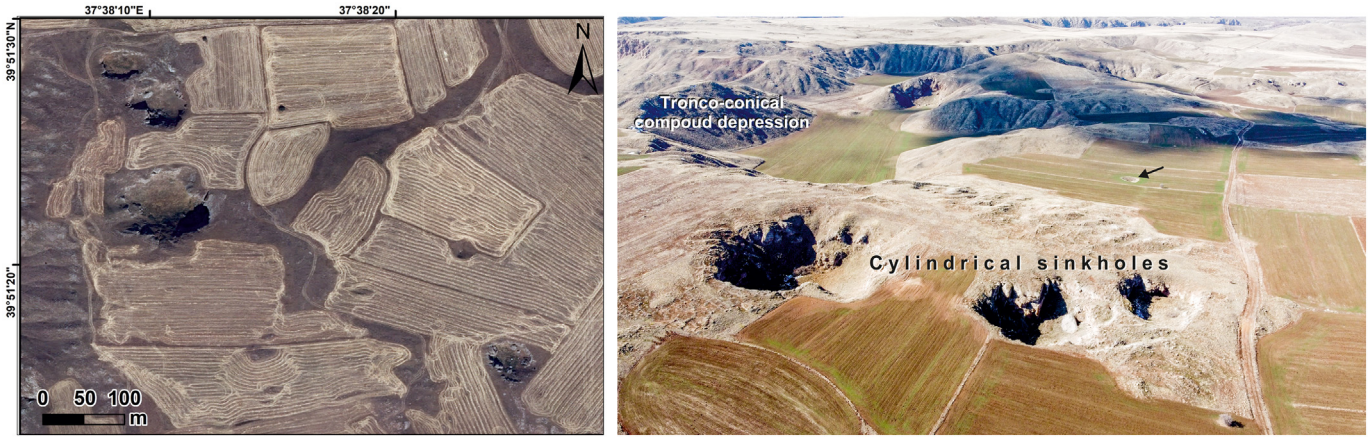

Fig. 6. Images of recent bedrock collapse sinkholes with cylindrical geometry located N of Tödürge canyon. Black arrow points to ponor.

swallow holes or springs (Fig. 5). Two main groups of depressions can be differentiated: 256 single sinkholes and 39 compound depressions related to the coalescence of two or more adjacent bedrock collapse sinkholes. The morphometric features of the two groups are analysed separately (Table 1).

The single bedrock collapse sinkholes display a complete morphological gradation, from relatively small, scarp-edged cylindrical holes to large depressions with a tronco-conical geometry and gentle slopes. This morphological spectrum reflects the different evolutionary stages of the sinkholes and their relative age. The young, fresh-looking cylindrical sinkholes are characterised by a subcircular perimeter and subvertical to overhanging gypsum cliffs affected rock-falls and topples (Fig. 6). Their margins often display arcuate dilated cracks providing evidence of incipient mass movements. Their floors show gypsum blocks related to the collapse of the cavity roof and subsequent mass wasting processes acting on the steep margins. The major axis of these cylindrical sinkholes ranges from 25 to 121 m and they have an average depth of 11 m.

The conical sinkholes are characterised by a flat bottom underlain by clayey deposits (i.e. insoluble residue), commonly used for cultivation, and sloping margins with variable angles largely depending on the degree of degradation (Fig. 7). Some conical depressions display rather steep margins with exposed gypsum bedrock, locally showing evidence of mass movements (Fig. 7E). In numerous cases, the relatively steep gypsum side slopes are dissected by gullies with centripetal arrangement (Fig. 7B). These gullies can head at the crest of the slope and modify the perimeter of the depression to form a crenulated outline. The more evolved conical sinkholes show more gentle slopes covered by colluvium and lacking bedrock exposures, which can be occupied by crop fields. Some conical sinkholes show marked asymmetry, with gentle slopes on one side and steeper slopes on the opposite side (Fig. 7D). In a number of cases this geometry seems to be controlled by the dipping structure of the bedrock. The single conical sinkholes reach a diameter of 634 m and have an average depth of 26 m.

The morphological gradation presented above shows that bedrock collapse sinkholes experience throughout their evolution a progressive increase in diameter and area but apparently there is not a depth decrease related to sediment accumulation from material shed from the side slopes. The outward expansion of the sinkhole edges eventually leads to the coalescence of nearby sinkholes and the formation of compound depressions. The overall morphometric parameters of the single sinkholes are presented in Table 1. They have an average major axial length of 213 m, high elongation and circularity ratios (0.85–0.86) and an average depth of 26.2 m. Some sinkholes due to their topographic location have an anomalously high depth, which is defined as the vertical distance between the deepest point of the floor and the highest point of the edge. This is the case of Büyükkörmen (125 m deep), Bölükbaşı (116 m deep), Serki and Uzun sinkholes, which intersect the slopes between the Low Plateau Surface and the High Plateau Surface (Fig. 5).

The compound sinkholes include the largest and morphologically more complex depressions. They are mainly related to the coalescence of degraded single conical sinkholes, can show a highly irregular perimeter and may include disconnected floors and at different elevations. Silgin depression, located to the SE of Tödürge Lake, is the largest compound sinkhole (Fig. 7A). It covers an area of 1.3 km^2, has a major axis of 1912 m and an estimated volume of 26 10^6 m^3. This depression is related to the coalescence of two sinkhole alignments with ENE and NE trends and is in the process of merging with other adjacent sinkholes on the NE, SW and ENE edges. The bottom of this depression, lying at an elevation similar to that of the water table, hosts lakes that drain through natural and artificial channels towards Tödürge Lake. At the foot of the slope in the NE margin of the depression there are two springs that discharge water from the gypsum karst aquifer and feed the lake (Fig. 7A).

The westernmost Lota sinkholes east of Hafik provide an example of the sequential collapse and coalescence of several single sinkholes, showing different degrees of degradation (Fig. 7E). They form a linear NE-SW-oriented belt associated with the northern margin of the Kızılırmak River valley. The eastern compound depression results from the coalescence of three adjacent sinkholes. The northeastern portion corresponds to a former single sinkhole with subcircular perimeter and a permanent lake. It shows a high degradation degree, with gentle northern slopes and relatively steep southern slopes with evidence of active mass movements. The southern portion with elongated geometry and around 80 m across results from the coalescence of two relatively small sinkholes related to the collapse of a NNE-oriented cave. This sector of the depression shows fresh-looking scarped margins and connects at its southern edge with an adjacent single collapse sinkhole through a non-collapsed cave section that forms a natural bridge

Fig. 7. Drone images of single and compound bedrock collapse sinkholes. Red arrows point to bedrock collapse sinkholes (A) Silgin depression is the largest compound sinkhole. Calcium-sulphate springs in the foreground. Tödürge Lake in the background. (B) Aşağıekinli sinkhole 360 m across showing a mature stage of development. The margin has been partially eroded by the Kızılırmak River, but still remains as an enclosed depression. (C) Kırdavut compound sinkholes captured by a stream and integrated into the surface drainage. (D) The asymmetric Sakşakkaya sinkhole, with very degraded side slopes, except in a small section with steep gypsum cliffs affected by mass movements. Blue arrow points to car for scale. (E) Lota sinkholes illustrating the progressive collapse of a cave section and the coalescence of the resulting sinkhole alignment. Blue arrow points to car for scale.

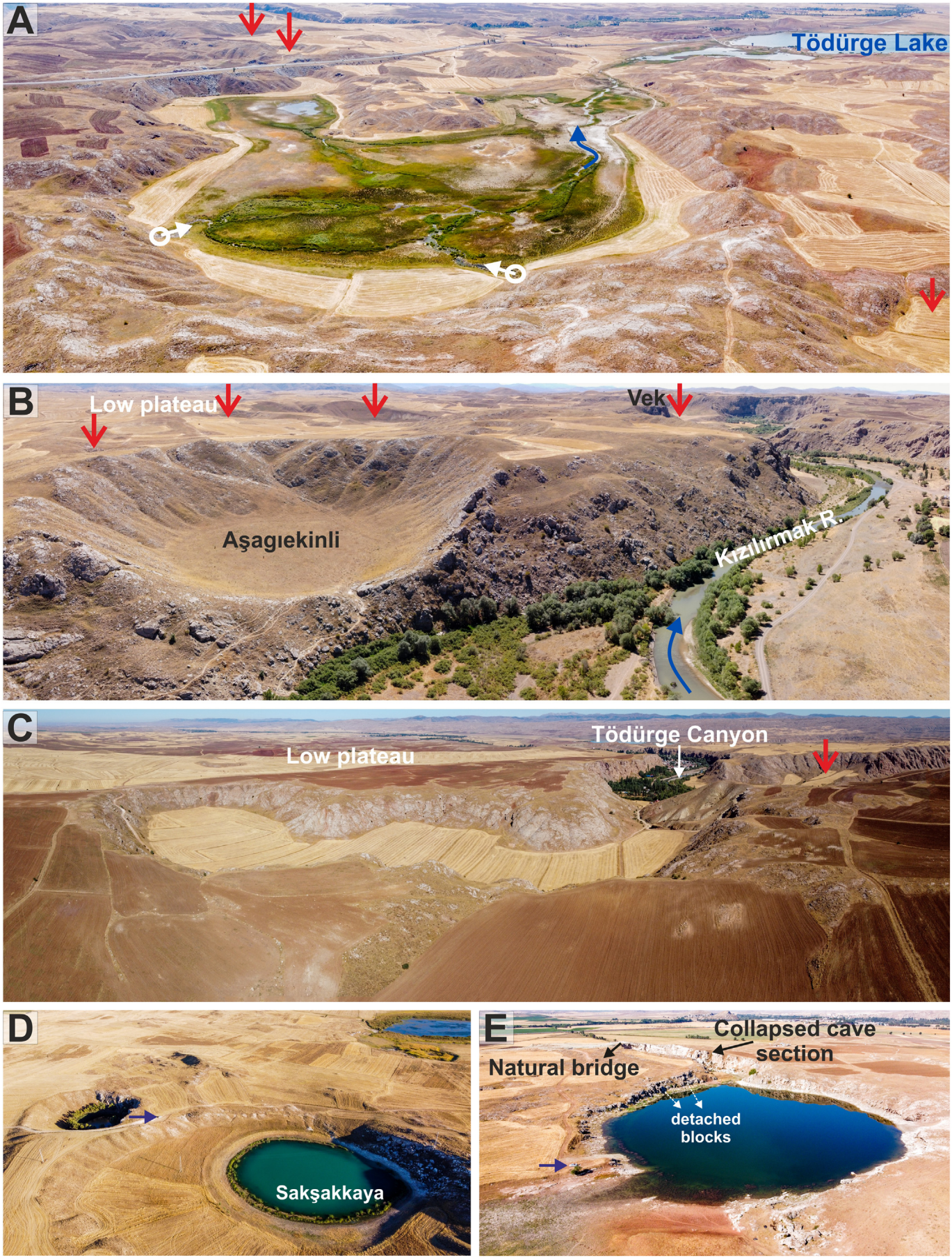
A
Tödürge Lake
B
Low plateau
Vek
Aşagıekinli
Kızılırmak R.
C
Low plateau
Tödürge Canyon
D
Sakşakkaya
E
Collapsed cave section
Natural bridge
detached blocks

(Fig. 7E). Collapse and slope instability processes will integrate this young sinkhole into the compound sinkhole located to the north. Around 35 m to the south there is another recent collapse sinkhole attributable to the same cave passage. This sinkhole alignment illustrates the successive collapse of cave sections from NE to SW and the coalescence of the collapse sinkholes as they increase their area due to mass wasting and water erosion processes acting on their margins. The main morphometric parameters of the compound bedrock collapse sinkholes clearly show that they correspond to a distinctive evolutionary group. Their average major axis (518 m) and area (171.661 m^2) are 143% and 327% larger than those of the single sinkholes. They also have significantly lower circularity and elongation ratios; 0.66 and 0.74, respectively.

A number of sinkholes, both single and compound, have been cut by the Kızılırmak River valley, especially along the Tödürge Canyon (Fig. 5). In some of them the erosion has partially removed their margins but remain as enclosed depressions (e.g., Aşağıekinli sinkhole; Fig. 7B), whereas others have been opened and integrated into the surface drainage network (e.g., Vekçukuru sinkhole, Kırdavut sinkhole; Fig. 7C). Waltham et al. (2005) suggested that collapse sinkholes get older with distance from the main drainages. Although this is the inferred trend at the Lota sinkholes described above, the production of a comprehensive cartographic sinkhole inventory reveals that there is not a clear temporal pattern at the margins of the Kızılırmak River. For instance, the Sakşakkaya sinkhole 300 m in length and located close to the Kızılırmak River shows a mature stage with highly degraded margins, except in a small steeper section affected by mass movements (Fig. 7D). Moreover, the recent cylindrical sinkholes display a rather scattered distribution and in some areas sinkholes showing a wide range of morphological stages occur spatially associated forming clusters. A good example is provided by the sinkhole group east of Mahmutagaçiftligi, at the northern margin of the Acısu Canyon.

The rose diagram inset in Fig. 4 shows the frequency distribution of the orientation of the major axis of all the bedrock collapse sinkholes. Despite the bedrock has a prevalent E-W trending structural grain related to the N-S compression associated with the tectonic inversion of the Sivas Basin, this orientation shows the lowest values. The azimuths display a wide distribution with a primary NW mode and a secondary NE mode. The aggregate volume of the bedrock collapse sinkholes, including both single and compound depressions, reaches 284,151,805 m^3. This value, together with the area of the minimum bounding polygon embracing the bedrock collapse sinkholes (1072.4 km^2), yields an average surface lowering of 0.26 m related to the suite of processes involved in the development of the depressions, discussed below. The surface lowering rises to around 0.70 m if we restrict the area to the LPS at the margins of the Tödürge Canyon, where sinkholes reach the highest density. Nonetheless, at the present time the cave-collapse process responsible for the initial development of the bedrock collapse sinkholes seems to have a limited geomorphic impact as reveals the available historical imagery. Detailed examination of the aerial photographs taken in 1966 indicate that no new bedrock collapse sinkholes have formed since that date, yielding a probability of occurrence lower than 1.69 10^{-5} sinkholes/km^2/yr.

The spatial distribution of the bedrock collapse sinkholes in the Sivas gypsum karst displays three remarkable features: (1) The majority of them, 268 out of 295 (91%), occur in the Low Plateau Surface (LPS), whereas the High Plateau Surface (HPS) is riddled by tightly packed solution sinkholes that form a striking polygonal karst landscape (Figs. 4, 5). The density of bedrock collapse sinkholes in the LPS and the HPS are 0.9 and 0.08 sinkholes/km^2, respectively. (2) The highest density occurs at the margins of the Tödürge Canyon, where the Kızılırmak River valley is deeply entrenched into the gypsum bedrock. High density is also observed on the southern margin of the Kızılırmak River valley south of Canova (Fig. 4). This is illustrated by the Kernel density model generated with the centroid of the depressions shown in Fig. 8. (3) Sinkholes display a markedly clustered distribution. A Nearest Neighbour Index

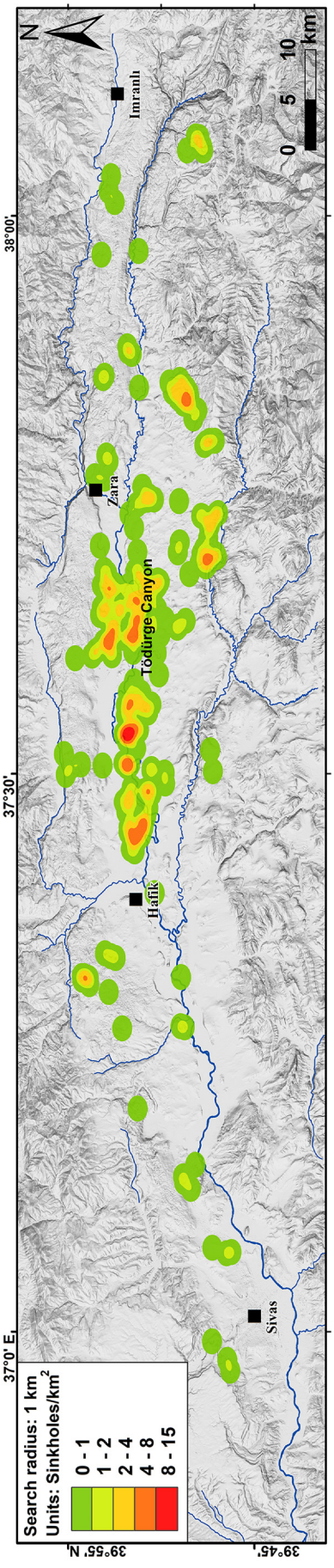

Fig. 8. Kernel density model generated with the centroid of the bedrock collapse sinkholes, showing their highly clustered distribution. Note high concentration of sinkholes associated with the Tödürge Canyon, mainly on its northern margin.

(NNI) of 0.44 indicative of high clustering has been computed for the study area, with a z-score of ~18.77 and a *p*-value of 0.0. This index, widely used in sinkhole investigation (Gutiérrez, 2016 and references therein), quantifies the degree of clustering versus scattering of sinkholes in a certain area and varies from 0 to 2.15. A NNI of 2.15 indicates maximum dispersion with hexagonal pattern, 1 perfect random distribution and 0 indicates maximum clustering (no separation between each sinkhole of the population and the nearest one).

The frequency-size relationships of the 256 single and the 39 compound bedrock collapse sinkholes is described plotting their major axis (Ma), area (A) and volume (V) in logarithmic scale against cumulative frequency (Fc; proportion of sinkholes with a dimension equal or larger than a given size value) (Fig. 9). Note that those parameters do not correspond to the size of the depressions at the time of formation, but to dimensions attained after a variable time span of morphological modification by multiple processes non-related to subsidence (e.g. max wasting, erosion). The graphs show the range covered by the computed values and allow comparing the size distributions of different sinkhole groups. The empirical data in all cases show a general linear trend in the semi-log graph that can be fitted with a high

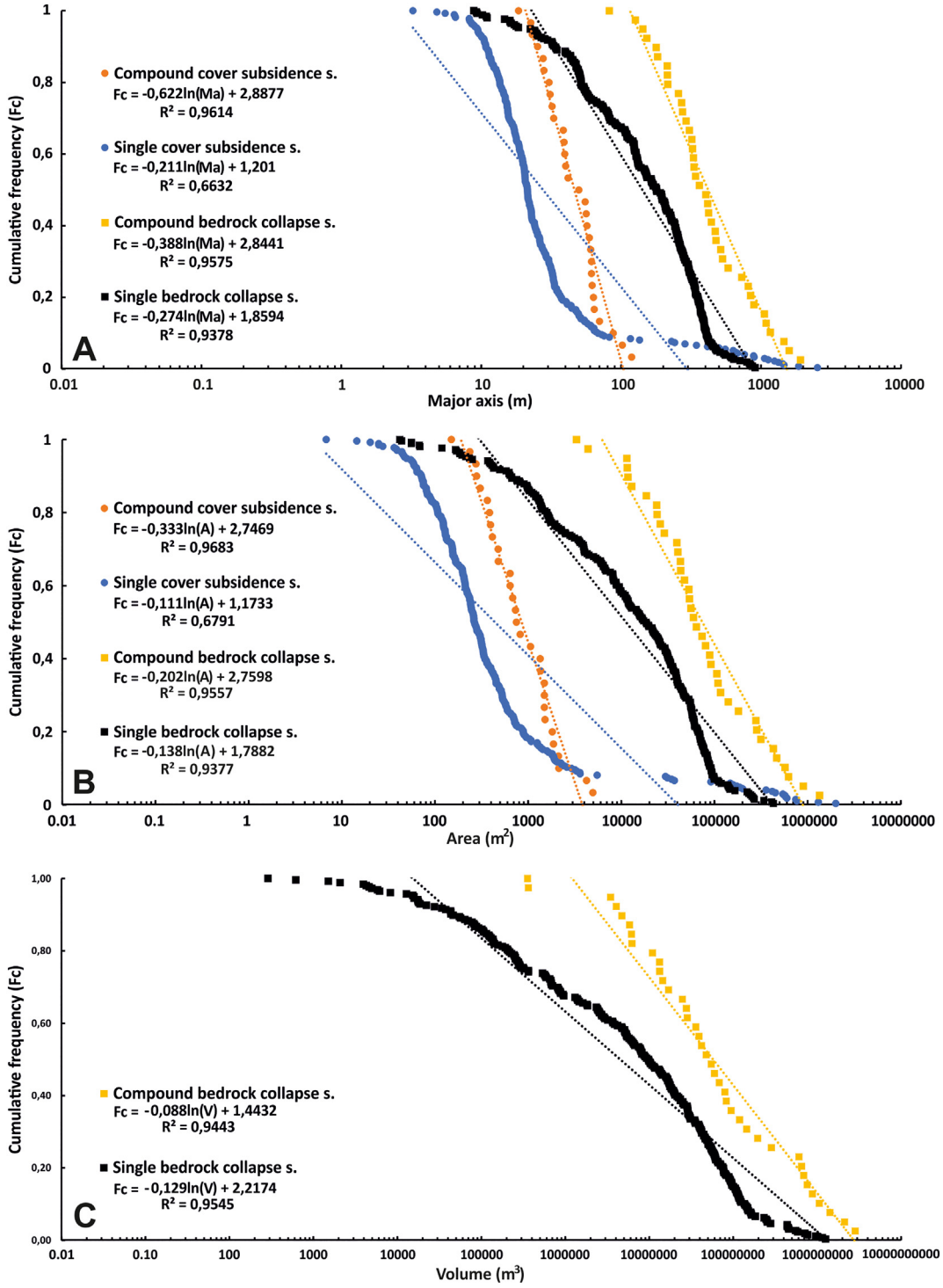

Fig. 9. Frequency-size relationships constructed with the major axis (A), area (B) and volume (C) of the inventoried single and compound bedrock collapse sinkholes and cover subsidence sinkholes.

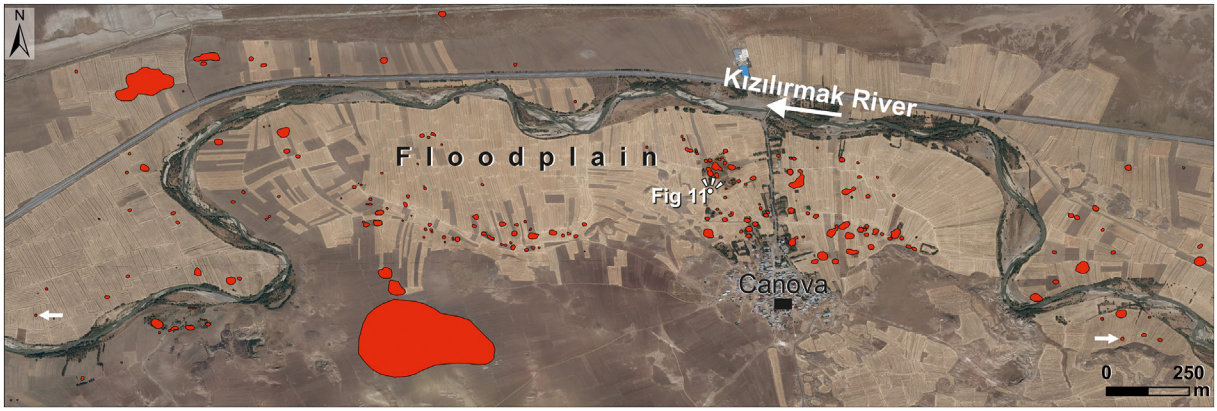

Fig. 10. Distribution of the cover subsidence sinkholes mapped in the stretch of the Kızılırmak River valley where they display the highest density. Arrows point to sinkholes formed between 1973 and 2015.

goodness of fit with logarithmic functions, with correlations coefficients above 0.93. The dimensions of the major axis, area and volume of single bedrock collapse sinkholes cover 2.0, 4.0 and 6.6 orders of magnitude, given by log (maximum value/minimum value). The corresponding orders of magnitude for the compound bedrock collapse sinkholes are 1.9, 3.6 and 3.9, respectively.

4.2.2. Cover subsidence sinkholes

A total of 302 cover subsidence sinkholes have been mapped, 38 of which correspond to buried sinkholes filled by farmers. These depressions mainly occur in crop fields on the floodplain and lower terraces of the Kızılırmak River (Figs. 10, 11). Here, the alluvium overlying the gypsum bedrock mainly consist of fine-grained clayey sand facies and locally reaches as much as 30 m (Drahor, 2019). This high thickness can be attributed, like in many other gypsum karst areas, to dissolution-induced synsedimentary subsidence and the presence of alluvium-filled paleosinkholes and subsidence basins (Gutiérrez and Cooper, 2013 and references therein). The mapped cover sinkholes reach an aggregate area of 9.58 km^2. Considering the area of the minimum bounding polygon that embraces all the cover sinkholes (586.25 km^2), they yield density values by number and percentage area of 0.52 sinkholes/km^2 and 1.63%, respectively. These should be considered as minimum values since a significant number of sinkholes may have been obliterated by human activity and natural processes (e.g. aggradation during floods). At least 19 sinkholes can be confidently classified as cover collapse sinkholes based on their well-defined scarped edges. The rest of the sinkholes with diffuse edges could be related to sagging, suffosion, collapse or a combination of these mechanisms. Note that the marginal scarps of the collapse sinkholes underlain by unconsolidated cover deposits can experience rapid degradation and depressions can rapidly acquire the appearance of sagging or suffosion sinkholes (i.e., morphologic convergence or equifinality). A significant proportion of the cover sinkholes, with their bottom situated at or close to the water table, host permanent or ephemeral lakes (Fig. 11).

The cover subsidence sinkholes can be also divided into 272 single depressions and 30 compound depressions related to the coalescence of adjacent sinkholes. The morphometry of these two groups has been analysed separately (Table 2). Single cover sinkholes have an average major axis and an average area of 21.8 m and 670 m^2, respectively, whereas the corresponding values for compound depressions are 50 m and 1162 m^2, respectively, around two times higher. Circularity and elongation ratios of single depressions (0.93, 0.87) are significantly higher than those of the compound depressions (0.70, 0.72).

The frequency-size relationships of the 275 single and the 27 compound cover subsidence sinkholes are described plotting their major axis (Ma) and area (A) against cumulative frequency (Fc) in a semi-log graph (Fig. 9). The computed dimensions show a linear trend for

Fig. 11. Clusters of cover subsidence sinkholes forming large compound depressions in the Kızılırmak River floodplain (see location in Fig. 10). Black arrows point to sinkholes filled by farmers, recognisable by a darker tone and a subtle depression.

Table 2
Main morphometric parameters of the single and compound cover subsidence sinkholes extracted from the cartographic inventory.

Parameter	Single sinkholes				Compound sinkholes			
	Maximum	Minimum	Average	Standard deviation	Maximum	Minimum	Average	Standard deviation
Major axis (m)	2530.29	3.24	93.08	284.80	118.75	18.47	49.99	23.29
Circularity ratio	0.98	0.61	0.93	0.04	0.94	0.46	0.70	0.14
Elongation ratio	0.98	0.61	0.87	0.06	0.87	0.55	0.72	0.08
Area (m^2)	2,005,270.60	6.80	35,086.83	176,774.38	4936.70	149.96	1162.61	1091.04
Perimeter (m)	6642.64	9.58	72.19	751.78	293.02	48.46	133.35	59.49
Depth (m)	5.85	0.01	1.13	3.76	0.01	3.69	0.97	0.93

the compound cover subsidence depressions and can be described by logarithmic functions with correlation coefficients higher than 0.96. In contrast, the depressions ascribed to the single category show a very broad size distribution and a relatively poor correlation with the regression curve (R^2: 0.66–0.68). The values of the major axis of the compound and single depressions cover 0.8 and 2.9 orders of magnitude. The area ranges for the compound and single sinkholes encompass 1.5 and 5.5 orders of magnitude. These features support the concept that the cover subsidence group includes different genetic types (collapse, suffossion, sagging) and that probably some large subcircular sinkholes interpreted as single could correspond to compound depressions.

Cover subsidence sinkholes show a marked high spatial frequency in the area around Canova village, where 152 of the inventoried sinkholes occur, around 50% of the total. Here, in an area covering 3.2 km^2 the sinkhole densities by number and area reach 47.5 sinkholes/km^2 and 6.3%, respectively (Fig. 10). The density of sinkholes shows a general increase towards the valley margin, probably related to the wedging out of the alluvial cover, although this interpretation cannot be tested due to the lack of data on alluvium thickness. The distribution of cover subsidence sinkholes, similarly to bedrock collapse sinkholes, is strongly clustered, with a Nearest Neighbour Index (NNI) of 0.32, a z-score of ~22.6 and a *p*-value of 0.0. In some cases, clusters of tightly packed sinkholes merge forming large depressions as much as 180 m across with irregular perimeter and numerous nested sinkhole bottoms (Fig. 11). The interpretation of aerial photographs taken at different dates has allowed the identification of four cover sinkholes formed between 1973 and 2015 and one between 1966 and 1973. Two of the recent sinkholes are labelled in Fig. 10. In Sivas city area, aerial photographs show that at least three sinkholes have been buried and used for urban development.

4.3. Relict valleys

The Low Plateau Surface is carved by a swarm of linear depressions with a dominant NW-SE trend interpreted as relict valleys. These are remnants of an ancient drainage system and consequently important features for the paleohydrological reconstruction of the Sivas gypsum karst. They mainly occur in the plateau surface situated between the Kızılırmak River canyon and the Acısu River, and their forking and general slope indicate that they used to be tributaries of both drainages (Fig. 4). The relict valley sections are perched around 50 m above the Kızılırmak River and have an average depth of 33 m. The length of the mapped relict valley sections ranges from 0,17 to 8,6 km. The bottom of the valleys has been re-shaped by sinkholes, which interrupt their original graded longitudinal profile. Some of them also display active swallow holes or ponors (Fig. 12). Thus these valleys that used to convey the surface runoff towards the main drainages currently function as groundwater recharge features.

5. Discussion

5.1. General geomorphological and paleohydrological evolution

The Sivas gypsum karst displays a number of outstanding features compared with other gypsum-karst areas worldwide (Klimchouk et al., 1996b; Gutiérrez and Cooper, 2013): (1) extensive staircased planation surfaces cut-across deformed gypsum bedrock; (2) a remarkable polygonal karst with tightly packed solution sinkholes in the upper planation surface; (3) a high density of bedrock collapse sinkholes with exceptionally large dimensions in the lower planation surface; (4) peculiar deranged relict valleys in the lower planation surface; and (5) long and deeply entrenched canyons carved into the gypsum bedrock. (6) local high density of cover subsidence sinkholes. Proper understanding of these gypsum karst features and the current functioning of the system requires reconstructing the long-term geomorphic and paleohydrological evolution of the region.

The development of the bare gypsum karst essentially started sometime after the deposition of the Early Miocene marine limestone of the Karacaören Fm., and once the sediments overlying the Late Eocene Hafik evaporites were removed by erosion. The Late

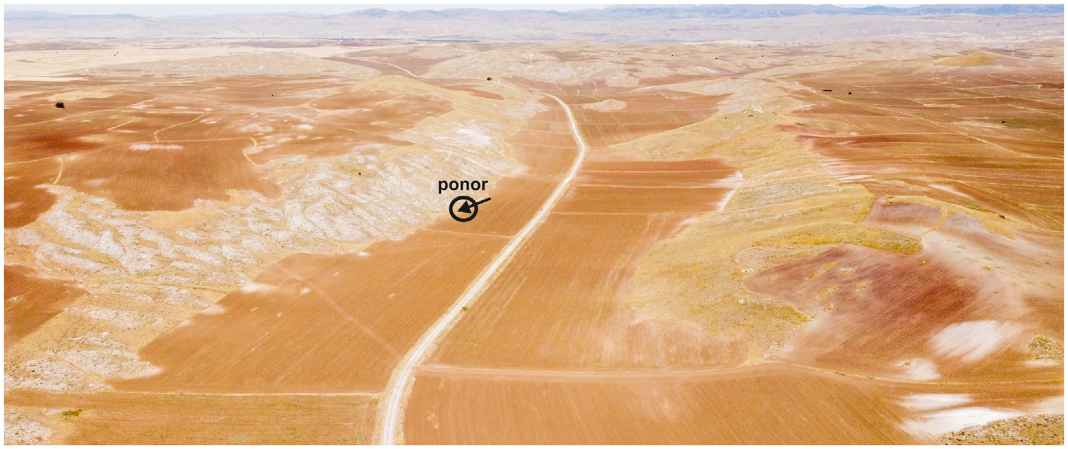

Fig. 12. The NW-SE oriented Tazıbel relict valley (see location in Fig. 5). Ponor on its edge.

Cenozoic evolution of the landscape has occurred within a context of regional uplift and base level deepening, as proved by the current position of the Early Miocene marine limestones lying at 1400–1600 m a.s.l. The geomorphic record reveals two main phases of landscape development with contrasting denudational styles. The first phase, most probably controlled by a slow base-level drop interrupted by relatively long periods of stability, was dominated by the development of the two stepped planation surfaces corresponding to the High Plateau Surface and the Low Plateau Surface. The second phase is characterised by rapid fluvial downcutting and the excavation of deeply entrenched gypsum canyons.

The highest and oldest erosional surface (High Plateau Surface), inset with respect to the structural platform capped by the Late Pliocene Meraküm Fm., has a poorly constrained Late Pliocene-Quaternary age. During its development, the base level presumably remained at a relatively stable position and solutional and mechanical erosion processes created a nearly flat landscape with the water table situated close to the surface. During the subsequent base-level deepening episode, the planation surface became a relict surface perched above the base level and started to function as a major autogenic recharge zone for the karst hydrological system. In this flat surface underlain by highly soluble gypsum bedrock, a great proportion of the precipitation water infiltrates and causes the differential dissolution of the bedrock. This long-sustained process of dissolution by percolating vadose water within the epikarst has resulted in the development of the tightly packed solution sinkholes (polygonal karst) that display the High Plateau Surface (e.g. Williams, 1972). The base level experienced a subsequent episode of stability in the Pleistocene, recorded by the Low Plateau Surface, inset around 100–200 m below the High Plateau Surface. Sometime in the Pleistocene, the Kızılırmak River, which functions as the regional base level for the karst system, together with its tributary the Acısu River, rapidly incised into the Low Plateau Surface, which also became an additional autogenic recharge area. During the initial phase of fluvial incision, a tributary drainage network was carved into the Low Plateau Surface between both drainages. This was probably a period of higher effective precipitation in which fluvial activity overwhelmed karst processes that tend to hamper surface drainage (e.g. diffuse and focused infiltration, formation of collapse sinkholes). As fluvial entrenchment progressed, together with the associated water-table drop, cave systems developed in the gypsum bedrock controlled by the declining water table. The bedrock collapse sinkholes mainly distributed in the Low Plateau Surface provide indirect evidence for those caves that essentially remain undiscovered. Karstification and subsidence in the Low Plateau Surface eventually caused the disruption of the ancient tributary valleys developed between the Kızılırmak and Acısu rivers, transforming them into linear depressions with internal drainage.

5.2. Sinkhole distribution and development

The Sivas gypsum karst displays a remarkable diversity of sinkholes with well-defined spatial distribution: (1) solution sinkholes mainly in the High Plateau Surface; (2) bedrock collapse sinkholes mostly located in the Low Plateau Surface at the margins of the regional base level (Tödürge Canyon of the Kızılırmak River); and (3) cover subsidence sinkholes associated with the floodplain and low terraces of the Kızılırmak River. The hydrogeological context in which these sinkholes have developed essentially corresponds to an unconfined karst aquifer with autogenic recharge in the perched E-W-oriented planation surfaces (epigene system) and a regional underground flow towards the longitudinal drainages that function as base levels and as the main groundwater discharge zones. The main springs area associated with the Kızılırmak River valley. The existence of hypogene groundwater circulation can be discarded due to the fact that gypsum formation is underlain by very low permeability units (turbidites of the Bozbel Fm). The extent and distribution of the main recharge zones changed through time as the two erosional surfaces successively became perched due to base level deepening. Coevally, the water table declined increasing the thickness of the vadose zone and most probably controlling the development of multi-level cave systems with passages at progressively lower elevations.

The sinkhole types observed in the High and Low Plateau surfaces are markedly different despite they are underlain by the same lithology. This sinkhole zonation can be attributed to the hydrogeological position of the different areas. The High Plateau Surface is the highest and oldest recharge area dominated by water infiltration and downward vadose zone, which has created over a long period of time an exceptionally well-developed polygonal karst. This zone is less favourable for the formation of bedrock collapse sinkholes, since the phreatic zone is located at significant depth and the flow rate in the aquifer is comparatively low due to the limited contributing area. The computed densities of bedrock collapse sinkholes in the High and Low Plateau Surfaces are 0.08 and 0.9 sinkholes/km^2, respectively. The fact that bedrock collapse sinkholes are mainly concentrated on both sides of the Tödürge Canyon, and especially on its northern margin, can be attributed to the following factors: (1) These sectors close to the discharge zone have larger contributing area, greater groundwater flow rate and therefore more favourable hydrological conditions for the development of caves. In contrast with carbonate karst systems, groundwater in gypsum aquifers can flow for long distances before it reaches saturation conditions; (2) The greatest groundwater flow is expected to occur on the northern margin of the Kızılırmak River, downflow of the High Plateau Surface, which is the main recharge zone; (3) The water table depth and thickness of the vadose zone in the Low Plateau Surface is much lower, increasing the probability for collapsing cavities to intercept the surface. The solution sinkholes that form the polygonal karst in the High Plateau Surface, as expected for karst features related to groundwater recharge on a relatively flat surface, are widely distributed forming a tightly packed network of depressions. In contrast, both bedrock collapse sinkholes and cover subsidence sinkholes display a highly clustered distribution with Nearest Neighbour Indexes of 0.44 and 0.32, respectively. This spatial pattern can be attributed to the localized distribution of epigene caves responsible to the development of bedrock collapse sinkholes and probably also to areas of focused groundwater discharge in the bottom of the Kızılırmak River. The major axes of the bedrock collapse sinkholes show a primary NW trend and a secondary NE one. These prevalent orientations suggest that the development of gypsum caves is controlled by a conjugate system of oblique fractures related to the N-S compressional tectonic regime. Relict valleys also display a dominant NW trend.

The Late Eocene Hafik Formation is a gypsum/anhydrite succession several hundred meters thick that at least locally includes significant halite units. The Celalli-1 oil-exploration well, located south of the investigated area traversed 89 m of halite at more than 2000 m depth (Onal et al., 2008). This well is located in a sector of the Sivas Basin with a complex salt-tectonics structure, including salt walls (i.e. elongated salt diapirs) and intervening salt-withdrawal basins (e.g. Kergaravat et al., 2016). An important issue is whether interstratal salt dissolution plays a significant role in the development of the sinkholes inventoried in this work. The lack of deep borehole data precludes answering this question with direct information, but hydrochemical data can provide relevant clues. Table 3 shows water analyses from the Sivas karst published by Günay (2002), plus gypsum and halite saturation indexes calculated for this work. The water samples were collected in: (1) springs on the northern margin of the Kızılırmak River NE of Sivas (Seyfe and Göydün springs with mean discharges of 0.25 and 1.15 m^3/s); (2) the West and East Lota lakes on the northern margin of the Kızılırmak River east of Hafik; (3) Tödürge Lake in the central sector of the area; and (4) the Kızılırmak River at Sivas and Kırıkkale, the latter located downstream of the evaporite area. These analyses indicate that (1) water is dominated by the Ca-sulphate hydrochemical facies; (2) the amount of halite dissolved, with contents estimated from the

Table 3
Chemical analyses of water samples collected in 16 August 2001. Data from Günay (2002) and saturation indexes (SI) of gypsum and halite calculated with PHREEQC and the database of thermodynamic data WATEQ4F. (Courtesy of Prof. Luis Auqué).

	Seyfe Spring	Göydün Spring	West Lota Lake	East Lota Lake	Tödürge Lake	Kızılırmak River (Sivas)	Kızılırmak River (Kırıkkale)
Temperature (°C)	13	13	24	26	25	29	24
EC (μS cm^{-1})	13,000	13,000	2700	300	8000	3600	1650
Na (ppm)	2377.5	2390.0	42.8	118.7	1181.0	326.0	179.0
K (ppm)	5.25	5.0	6.29	4.79	7.10	4.0	4.90
Ca (ppm)	570.0	575.0	462.5	485.0	515.0	345.0	120.0
Mg (ppm)	42.5	40.0	34.0	30.0	45.0	34.0	29.0
HCO_3 (ppm)	329.77	329.77	99.25	99.25	99.25	154.70	157.56
Cl (ppm)	3598.5	3704.53	42.54	164.84	1790.23	549.48	228.65
SO_4 (ppm)	1342.50	1242.50	1202.12	1230.96	1344.42	788.66	384.81
$\sum$ Anion (meq L^{-1})	134.5	135.78	27.86	31.91	80.12	34.46	17.05
$\sum$ Cation (meq L^{-1})	135.19	136.08	27.60	31.96	80.96	34.30	16.78
SI gypsum	−0.28	−0.31	−0.17	−0.17	−0.25	−0.46	−1.01
SI halite	−3.78	−3.77	−7.39	−6.37	−4.39	−5.42	−6.01

concentrations of chloride and sodium of ≤6 g L^{-1}, is well below the solubility of halite (424 g L^{-1}; solubility per litre of pure water); (4) waters are highly undersaturated with respect to halite and subsaturated with respect to gypsum. This information indicates that groundwater has experienced limited interaction with salt beds, characterised by a very rapid dissolution kinetics, and that karst development in the studied area is essentially related to gypsum dissolution. Probably significant halite units occur south of the investigated area, towards the depocenter of the basin and where salt tectonics dominates the geological structure (Kergaravat et al., 2016; Pichat et al., 2018; Ribes et al., 2018).

The large number of inventoried bedrock collapse sinkholes (256 single and 39 compound), which show a wide range of evolutionary stages, offer the opportunity to apply the ergodic concept by substituting time by space, in order to reconstruct their morphological evolution and infer the morphogenetic processes involved. Bedrock collapse sinkholes at their initial stages are characterised by cylindrical geometry and limited major axis and depth, with average values of 72 and 11 m, respectively. These scarped sinkholes evolve into much larger tronco-conical depressions with progressively more gentle slopes and larger diameters, that eventually can merge with other adjacent sinkholes forming compound depressions (Waltham, 2002; Doğan and Özel, 2005). Perhaps surprisingly, morphometric data also indicate that bedrock collapse sinkholes tend to increase their depth, despite one would expect that slope degradation should result in sediment aggradation and depth decrease. The fresh-looking cylindrical sinkholes have an average depth of 11 m, whereas the whole population of single bedrock collapse sinkholes have a mean depth of 26.2 m. The following evolution is proposed for the bedrock collapse sinkholes based on field observations and morphometric data, and supported by the high solubility of gypsum (2.6 g L^{-1}), which can be readily dissolved and evacuated as solute load by groundwater flow (Fig. 13): (A) Phreatic passages develop controlled by the position of the water table and with spans restricted by the groundwater flow rate and the limited mechanical strength of the gypsum. The largest known chambers in gypsum do not exceed 65 m (e.g. Harz Mountains, Germany; Kempe, 1996), whereas caverns developed in massive limestone can reach hundreds of meters across (e.g. Sarawak Chamber in Gunung Mulu National Park, Sarawak, Malaysia, is around 700 m long; Waltham, 2004). (B, C) Base level deepening and the associated water table drop favours the collapse of cavity roofs by buoyancy loss. Downward percolation of water in the vadose zone also contributes the reduce the rock mass strength by dissolution acting along discontinuity planes. The roof of the cavities propagates upwards by progressive roof collapse (stoping) until they reach the ground surface. A sinkhole with steep to overhanging walls and moderate size forms, which bottom is underlain by a chaotic openwork breccia of gypsum blocks (chaotic packbreccia). These breakdown deposits can form breccia pipes of significant thickness, depending on the depth of the cavity responsible for the creation of the sinkhole. (D) The steep scarped margins of the bedrock collapse sinkholes experience rapid degradation by mass wasting processes, favoured by the development of unloading cracks and the reduction of the internal friction of potential failure planes by gypsum dissolution. The margins of the sinkhole attain a sloping attitude and rock fall deposits accumulate on top of the cave-roof collapse breccia. (E) Once the side slopes of the sinkhole reach the repose angle, the development of mass wasting processes ceases and the slopes are mainly degraded by mechanical erosion through gullying and sheet wash, as well as by solutional denudation. The latter process can reach high rates in gypsum exposures even under semiarid climates (Desir et al., 1995). A large data set from Italy of dissolution rates in gypsum directly exposed to precipitation indicate that a cumulative rainfall of 500 mm is expected to cause a surface lowering of 0.56 mm a^{-1} (Klimchouk et al., 1996a). Shaw et al. (2011), using standard gypsum tables in the Gypsum Plain of the Delaware Basin (New Mexico and Texas) with an average annual precipitation of 270 mm, obtained an average surface denudation rate of 0.3 mm a^{-1}. The gypsum sediment shed from the sides of the sinkholes by mechanical erosion processes are temporarily accumulated in the bottom of the depressions. However, percolation water causes the progressive solutional removal of the deposits underlying the sinkhole floor, including the uppermost water-laid sediments and the thick gypsum breccia. This process of subsurface mass removal by vadose percolation increases its effectiveness as the sinkholes increase their diameter and the runoff contributing area enlarges. Moreover, the enlargement of sinkholes with lakes can be encouraged by lateral dissolution at the foot of their side slopes and the consequent basal retreat. As a result, the angular and porous chaotic packbreccia progressively transforms into a thinner floatbreccia consisting of highly corroded gypsum particles embedded within a residual clayey matrix enriched in the insoluble components of the Hafik Formation. This type of solutional transformation of gypsum breccias and the associated mass depletion has been documented in the evaporite karst of the Ebro River valley in Spain (Guerrero et al., 2013). The slow but continuous dissolution of the gypsum deposits and probably also the gypsum bedrock underlying the sinkhole bottom by increasing water percolation leads to the progressive deepening of the floor of the sinkholes. (F, G) As the side slopes degrade and decrease their inclination, they tend to be covered by colluvium transported by sheet wash and the sinkhole floor tends to increase its width. Mechanical erosion becomes progressively less important, but solutional removal of gypsum deposits and bedrock tends to increase together with the enlargement of the sinkhole acting as a precipitation collector. As explained above, the large diameter and depth of the mature bedrock collapse sinkholes are largely related to long-sustained solutional removal of gypsum starting from a relatively small depression created by cave collapse, which functions as a groundwater absorption feature. Consequently, the inferred surface lowering at the mature sinkhole sites can be primarily attributed to surface and near-surface chemical erosion and secondarily to subsidence by cavity collapse.

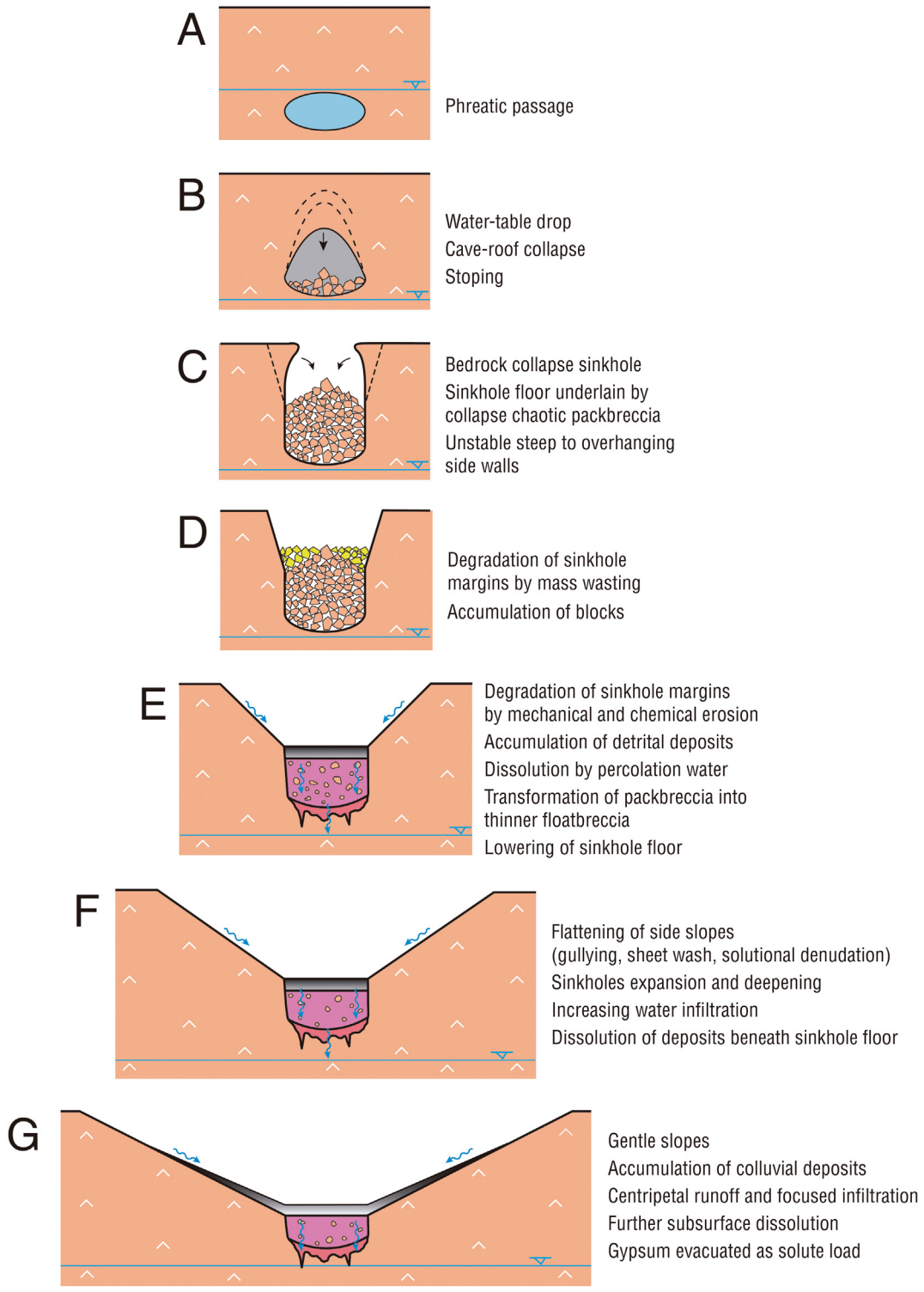

Fig. 13. Sketch illustrating the morphological evolution proposed for the bedrock collapse sinkholes, involving substantial post-collapse mass removal as solute load derived from by surface and subsurface dissolution of high-solubility gypsum.

The morphometric data obtained from the inventoried bedrock collapse sinkholes and cover subsidence sinkholes can be used to generate frequency-size relationships and compare them with those from other karst settings, in order to extract genetic and evolutionary inferences. The graph of Fig. 14 includes the relationship between cumulative frequency and the major axis of sinkholes inventoried in Sivas and other regions with diverse conditions (carbonate vs evaporites, epigene vs hypogene, different sediments covering the karst rocks): (1) limestone karst covered by thin unconsolidated alluvium (Val d'Orleans, France; Gombert et al., 2015); (2) a mantled limestone karst covered by a thick cohesive cover (Hamedan Plains, Iran; Taheri et al., 2015); (3) a salt karst with a residual gypsum-rich caprock (Ambal salt pillow, Iran; Gutiérrez and Lizaga, 2016; Jalali et al., 2019): (4) an epigene evaporite karst with both unconsolidated covers and lithified caprocks

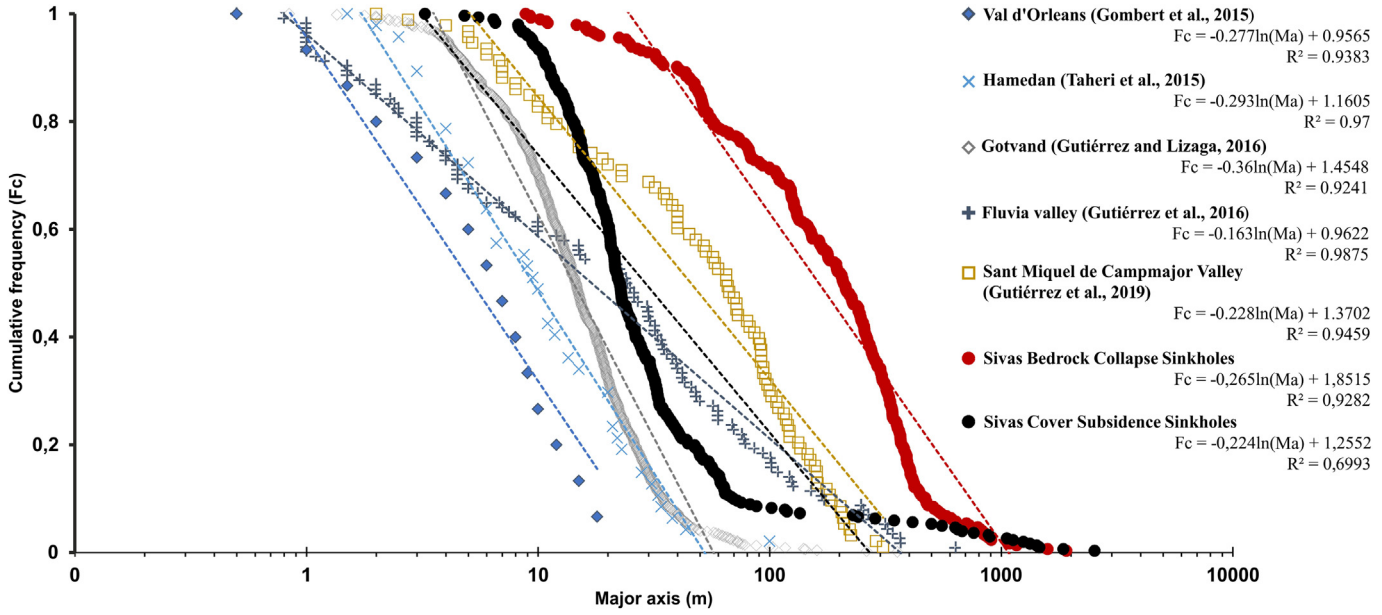

Fig. 14. Frequency and relationships constructed with the major axis of the inventoried sinkholes in the Sivas gypsum karst and different karst setting.

(Fluvia Valley, NE Spain; Gutiérrez et al., 2016); (5) an hypogene and deep-seated interstratal evaporite karst (Sant Miquel valley, NE Spain; Gutiérrez et al., 2019). The data plotted from Sivas include all the bedrock collapse sinkholes and all the cover subsidence sinkholes, without differentiating between single and compound, like in the other data sets. Overall, the variable distribution of the major axis data shows that the dimensions of the sinkholes depend on: (1) the subsidence mechanism (sagging, collapse, suffusion); (2) the nature and mechanical strength of the sediments overlying the cavities (or karstification zone); (3) the depth of the cavities; and of special importance in Sivas (4) the potential expansion that the sinkholes may experience by mechanical and chemical erosion processes. The smallest sinkholes, as expected, are those developed in the mantled limestone karst of Val d'Orleans, where internal erosion of thin and mechanically weak cover deposits into the cavernous limestone bedrock creates cover collapse sinkholes. Perhaps unexpectedly, the bedrock collapse sinkholes from the Sivas gypsum karst show the greatest dimensions, even bigger than the large sinkholes developed in the deep-seated hypogene evaporite karst of Sant Miquel, where collapse structures penetrate through thick lithified marl formations. This apparently anomalous size distribution can be attributed to the old age of most of the sinkholes at Sivas and the significant growth that they have experienced by the degradation of the slopes and eventually the amalgamation of nearby sinkholes. The cover subsidence sinkholes apparently show an anomalous frequency-size distribution, with a very large size range (lower slope of the regression curve), and a low correlation coefficient of 0.81, compared with the rest of values above 0.94. This pattern can be attributed to the mixed nature of this data set, comprising sinkholes generated by multiple mechanisms, including sagging sinkholes that may reach very large dimensions regardless of the thickness and mechanical strength of the sediments affected by settlement.

The occurrence of sinkholes and the activity of the existing ones, especially the buried depressions, have the potential to cause both significant economic and social damage in the Sivas karst. The region includes large cities and towns (e.g. Sivas, ca. 380,000 inhabitants; Zara, ca. 23,000 inhabitants). It is also traversed by the main Europe-Asia highway between Ankara and Sivas and the pipeline from the Baku oilfields in Azerbaijan to the Turkish Mediterranean port of Ceyhan, which gives service since 2005 and has around 70 km of its route across gypsum karst near Sivas. The steel thickness of this pipe was increased to be able to span sinkholes as large as 44 m across (Waltham, 2008). Moreover, there is also a project to construct a high-speed railway between Sivas and Erzincan, which runs along 135 km upon gypsum bedrock. Critical hazard parameters include the probability of occurrence of sinkholes, the size of the sinkholes at the time of formation, and the rapidity of the subsidence processes, which largely depends on the deformation mechanism (slow sagging versus catastrophic collapse) (Gutiérrez, 2016). The constructed cartographic sinkhole inventory, including data from historical imagery, indicates that bedrock collapse sinkholes, despite their large damaging capability, have a very low probability of occurrence. No new sinkholes of this type have been reported since 1966 in an area covering 980 km^2, indicating a spatial-temporal probability below 1.69 10^{-5} sinkholes/km^2/yr. This value could rise significantly if conditions are changed by human activity (e.g. Gutiérrez et al., 2014). Cover subsidence sinkholes show a more restricted distribution associated with the valley floors and a larger probability of occurrence, although difficult to assess, since these depressions tend to be filled by farmers (i.e. incomplete sinkhole inventory). Detailed mapping of these sinkholes including historical imagery provides two benefits for the application of preventive hazard avoidance measures (e.g. Gutiérrez et al., 2011): (1) identification of the sinkhole-prone areas; and (2) delineation of the buried sinkholes. Examination of aerial photographs from different dates show that at least four sinkholes in Sivas city have been filled and incorporated in developed areas (Fig. 15).

6. Conclusions

The world-class gypsum karst of Sivas displays outstanding geomorphic features: (1) extensive staircased planation surfaces cut-across deformed gypsum bedrock; (2) a striking polygonal karst landscape; (3) areas with a very high density of exceptionally large bedrock collapse sinkholes; (4) uncommon long and deeply entrenched gypsum canyons; and (5) a peculiar network of relict valleys disrupted by sinkholes. The chronological development of these features has been constrained within the geomorphic and paleohydrological evolution of the region within a context of long-term regional uplift and base level deepening.

The geomorphic record allows the differentiation of two major phases of landscape development with contrasting denudation styles. In an initial phase, characterised by relatively long periods of base

Fig. 15. Images of sinkholes located SE of Sivas city taken on different dates. The 1966 aerial photograph shows two large sinkholes associated with cropfields. The 2019 image shows the current situation after the artificial fill of the sinkholes and structures constructed on the northern depression. The building overlapping the northern sinkhole corresponds to school.

level stability, two stepped denudation surfaces were carved in the folded gypsum bedrock of the Hafik Fm.: the Plio-Quaternary High Plateau Surface and the Quaternary Low Plateau surface. In the subsequent phase, rapid fluvial incision resulted in the development of gypsum canyons deeply entrenched into the Low Plateau Surface. The formation of the remarkable polygonal karst associated with the High Plateau Surface most probably started soon after the formation of this planation surface. The relict valleys excavated in the Low Plateau Surface and disrupted by sinkholes record the onset of the incision phase following the formation of this younger planation surface. The excavation of the gypsum canyons and the concomitant lowering of the water table was accompanied by the development of cave systems, mainly distributed beneath the Low Plateau Surface. Collapse processes acting in these undiscovered caves have produced the numerous bedrock collapse sinkholes mapped in the Low Plateau Surface.

The Sivas gypsum karst shows a large diversity of sinkholes with well-defined spatial distribution: (1) densely packed and widely distributed solution sinkholes in the High Plateau Surface; (2) numerous bedrock collapse sinkholes with clustered distribution in the Low Plateau Surface; and (3) cover subsidence sinkholes in the alluvium-covered valley floors with high densities in specific areas. This zonation of the sinkholes types is attributed to the hydrogeological functioning of the epigene karst system, dominated by autogenic recharge in the perched plateau surfaces. The polygonal karst is mainly associated with the more distant recharge area, where dissolution by vadose water in the epikarst dominates. The bedrock collapse sinkholes mainly occur close to the discharge areas, where the groundwater contributing area and discharge is sufficiently large for the formation of well-developed caves. Cover subsidence sinkholes are restricted to the mantled karst areas of the valley floors and probably strongly influenced by zones of major groundwater discharge.

The continuous morphologic spectrum displayed by the bedrock collapse sinkholes, ranging from relatively small cylindrical holes to large and generally deeper tronco-conical depressions, reflects the geomorphic evolution of these sinkholes, involving the degradation of the slopes by mass wasting and erosion processes. Mature sinkholes reach hundreds of meters in diameter, despite the largest known caverns in gypsum are <100 m in length.

The exceptionally large dimensions of the sinkholes and the inferred deepening is attributed to the solutional removal of large volumes of gypsum by downward vadose flows in these groundwater recharge features. Runoff and percolation water dissolve gypsum in the slopes and the deposits underlying the sinkhole floor, including collapse breccias. The solutional denudation process proceeds through a positive feedback mechanism that increases its geomorphic work as the area of the sinkhole grows. This evolutionary model is markedly different to that commonly described for bedrock collapse sinkholes in carbonate rocks, characterised by lower solubility and erodibility. In carbonate bedrocks the degradation of the sinkhole margins leads to the accumulation of deposits that are scarcely affected by solutional removal, reducing the depth of the depressions and inhibiting the degradation of the side slopes.

Multi-temporal remote-sensed data reveals that bedrock collapse sinkholes, despite their high density in some areas, have a very low probability of occurrence. Nonetheless, this hazard could significantly increase if natural conditions are modified by human activities conductive to enhance dissolution and subsidence processes. The spatial-temporal frequency of cover subsidence sinkholes is relatively high in the most susceptible areas. Significant subsidence damage most probably will occur in the near feature associated with buried sinkholes used for construction. Detailed cartographic sinkholes inventories produced using historical imagery and the application of preventive planning is proposed as a cost-effective risk mitigation measure.

Declaration of competing interest

The authors wish to confirm that there are no conflicts of interest associated with this publication and there has been no significant financial support for this work that could have influenced its outcome.

Acknowledgements

The work conducted by FG has been supported by project CGL2017-85045-P (Ministerio de Ciencia e Innovación, Spanish Government). The contribution by MF has been supported by the Slovenian Research Agency (research programme P6-0101; research project N1-0162). This paper is a part of the first author's Ph.D. Thesis.

References

Akbulut, G., 2011. A suggested geopark site: gypsum karst topography between Sivas-Zara. In: Efe, R., Atalay, I. (Eds.), Natural Environment and Culture in the Mediterranean Region-II. Cambridge Scholars Publishing, UK, pp. 137–148.

Akkiraz, M.S., Kangal, Ö., Erdem, N.Ö., Büyükmeriç, Y., Doğruöz, C., 2018. Palaeontological evidence and sedimentary facies in a lower Miocene (Aquitanian) succession from the Bingöl minibasin (Sivas Basin), Central Anatolia. Turk. J. Earth Sci. 27 (5), 329–348. https://doi.org/10.3906/yer-1710-20.

Alagöz, C., 1967. Sivas çevresi ve doğusunda jips karstı olayları, 175. Ankara Üniversitesi Dil ve Tarih-Coğrafya Fakültesi Yayını (126 pp).

Calaforra, J.M., Pulido-Bosch, A., 2003. Evolution of the gypsum karst of Sorbas (SE Spain). Geomorphology 50 (1), 173–180. https://doi.org/10.1016/S0169-555X(02)00213-1.

Callot, J.-P., Ribes, C., Kergaravat, C., Bonnel, C., Temiz, H., Poisson, A., Vrielynck, B., Salel, J.-F., Ringenbach, J.-C., 2014. Salt tectonics in the Sivas basin (Turkey): crossing salt walls and minibasins. Bull. Soc. Géol. France 185 (1), 33–42. https://doi.org/10.2113/gssgfbull.185.1.33.

Cater, J.M.L., Hanna, S.S., Ries, A.C., Turner, P., 1991. Tertiary evolution of the Sivas Basin, central Turkey. Tectonophysics 195 (1), 29–46. https://doi.org/10.1016/0040-1951(91)90142-F.

Chiba, T., Kaneta, S.-I., Suzuki, Y., 2008. Red relief image map: new visualization method for three dimensional data. Int. Arch. Photogramm. Remote. Sens. Spat. Inf. Sci. 37 (B2), 1071–1076.

Cooper, A.H., 1998. Subsidence hazards caused by the dissolution of Permian gypsum in England: geology, investigation and remediation. Geol. Soc. Lond. Eng. Geol. Spec. Publ. 15 (1), 265–275. https://doi.org/10.1144/gsl.Eng.1998.015.01.27.

Cooper, A.H., Gutiérrez, F., 2013. Dealing with gypsum karst problems: hazards, environmental issues, and planning. In: Shroder, J.F. (Ed.), Treatise on Geomorphology. Academic Press, San Diego, pp. 451–462 https://doi.org/10.1016/B978-0-12-374739-6.00106-8.

Cooper, A.H., Farrant, A.R., Price, S.J., 2011. The use of karst geomorphology for planning, hazard avoidance and development in Great Britain. Geomorphology 134 (1), 118–131. https://doi.org/10.1016/j.geomorph.2011.06.004.

De Waele, J., Piccini, L., Columbu, A., Madonia, G., Vattano, M., Calligaris, C., D'Angeli, I.M., Parise, M., Chiesi, M., Sivelli, M., Vigna, B., Zini, L., Chiarini, V., Sauro, F., Drysdale, R., Forti, P., 2017. Evaporite karst in Italy: a review. Int. J. Speleol. 46 (2), 137–168. https://doi.org/10.5038/1827-806X.46.2.2107.

Desir, G., Sirvent, J., Gutierrez, M., Sancho, C., 1995. Sediment yield from gypsiferous degraded areas in the middle Ebro basin (NE, Spain). Phys. Chem. Earth 20 (3), 385–393. https://doi.org/10.1016/0079-1946(95)00052-6.

Doğan, U., Özel, S., 2005. Gypsum karst and its evolution east of Hafik (Sivas, Turkey). Geomorphology 71 (3), 373–388. https://doi.org/10.1016/j.geomorph.2005.04.009.

Doğan, U., Yeşilyurt, S., 2004. Gypsum karst south of İmranlı. Cave Karst Sci. 31 (1), 7–14.

Doğan, U., Yeşilyurt, S., 2019. Gypsum karst landscape in the Sivas basin. In: Kuzucuoğlu, C., Çiner, A., Kazancı, N. (Eds.), Landscapes and Landforms of Turkey. Springer International Publishing, Cham, pp. 197–206 https://doi.org/10.1007/978-3-030-03515-0_6.

Drahor, M.G., 2019. Identification of gypsum karstification using an electrical resistivity tomography technique: the case-study of the Sivas gypsum karst area (Turkey). Eng. Geol. 252, 78–98. https://doi.org/10.1016/j.enggeo.2019.02.019.

Fidelibus, M.D., Gutiérrez, F., Spilotro, G., 2011. Human-induced hydrogeological changes and sinkholes in the coastal gypsum karst of Lesina Marina area (Foggia Province, Italy). Eng. Geol. 118 (1), 1–19. https://doi.org/10.1016/j.enggeo.2010.12.003.

Ford, D., Williams, P., 2007. Karst Hydrogeology and Geomorphology. John Wiley & Sons, Chichester.

Galve, J.P., Gutiérrez, F., Lucha, P., Guerrero, J., Bonachea, J., Remondo, J., Cendrero, A., 2009. Probabilistic sinkhole modelling for hazard assessment. Earth Surf. Process. Landforms 34 (3), 437–452. https://doi.org/10.1002/esp.1753.

Gökkaya, E., Tunçel, E., 2019. Natural and human-induced subsidence due to gypsum dissolution: a case study from Inandik, central Anatolia, Turkey. J. Cave Karst Stud. 81 (4), 221–232. https://doi.org/10.4311/2019es0105.

Gombert, P., Orsat, J., Mathon, D., Alboresha, R., Al Heib, M., Deck, O., 2015. Role des effondrements karstiques sur les desordres survenus sur les digues de Loire dans le Val D'Orleans (France). Bulletin of Engineering Geology and the Environment 74 (1), 125–140. https://doi.org/10.1007/s10064-014-0594-8.

Guerrero, J., Gutiérrez, F., Bonachea, J., Lucha, P., 2008. A sinkhole susceptibility zonation based on paleokarst analysis along a stretch of the Madrid–Barcelona high-speed railway built over gypsum- and salt-bearing evaporites (NE Spain). Eng. Geol. 102 (1), 62–73. https://doi.org/10.1016/j.enggeo.2008.07.010.

Guerrero, J., Gutiérrez, F., Galve, J.P., 2013. Large depressions, thickened terraces, and gravitational deformation in the Ebro River valley (Zaragoza area, NE Spain): evidence of glauberite and halite interstratal karstification. Geomorphology 196, 162–176. https://doi.org/10.1016/j.geomorph.2012.06.024.

Guezou, J.C., Temiz, H., Poisson, A., Gürsoy, H., 1996. Tectonics of the Sivas basin: the neogene record of the Anatolian accretion along the inner Tauric suture. Int. Geol. Rev. 38 (10), 901–925. https://doi.org/10.1080/00206819709465371.

Günay, G., 2002. Gypsum karst, Sivas, Turkey. Environ. Geol. 42 (4), 387–398. https://doi.org/10.1007/s00254-002-0532-0.

Gündoğan, I., Önal, M., Depçi, T., 2005. Sedimentology, petrography and diagenesis of Eocene–Oligocene evaporites: the Tuzhisar Formation, SW Sivas Basin, Turkey. J. Asian Earth Sci. 25 (5), 791–803. https://doi.org/10.1016/j.jseaes.2004.08.002.

Gutiérrez, F., 2016. Sinkhole hazards. In: Cutter, S.L. (Ed.), Oxford Research Encyclopedia of Natural Hazard Science. Oxford University Press, pp. 1–92 https://doi.org/10.1093/acrefore/9780199389407.013.40.

Gutiérrez, F., Cooper, A.H., 2013. Surface morphology of gypsum karst. In: Shroder, J.F. (Ed.), Treatise on Geomorphology. Academic Press, San Diego, pp. 425–437 https://doi.org/10.1016/B978-0-12-374739-6.00114-7.

Gutiérrez, F., Lizaga, I., 2016. Sinkholes, collapse structures and large landslides in an active salt dome submerged by a reservoir: the unique case of the Ambal ridge in the Karun River, Zagros Mountains, Iran. Geomorphology 254, 88–103. https://doi.org/10.1016/j.geomorph.2015.11.020.

Gutiérrez, F., Guerrero, J., Lucha, P., 2008. A genetic classification of sinkholes illustrated from evaporite paleokarst exposures in Spain. Environ. Geol. 53 (5), 993–1006. https://doi.org/10.1007/s00254-007-0727-5.

Gutiérrez, F., Galve, J.P., Lucha, P., Castañeda, C., Bonachea, J., Guerrero, J., 2011. Integrating geomorphological mapping, trenching, InSAR and GPR for the identification and characterization of sinkholes: a review and application in the mantled evaporite karst of the Ebro Valley (NE Spain). Geomorphology 134 (1), 144–156. https://doi.org/10.1016/j.geomorph.2011.01.018.

Gutiérrez, F., Parise, M., De Waele, J., Jourde, H., 2014. A review on natural and human-induced geohazards and impacts in karst. Earth Sci. Rev. 138, 61–88. https://doi.org/10.1016/j.earscirev.2014.08.002.

Gutiérrez, F., Mozafari, M., Carbonel, D., Gómez, R., Raeisi, E., 2015. Leakage problems in dams built on evaporites. The case of La Loteta Dam (NE Spain), a reservoir in a large karstic depression generated by interstratal salt dissolution. Eng. Geol. 185, 139–154. https://doi.org/10.1016/j.enggeo.2014.12.009.

Gutiérrez, F., Fabregat, I., Roqué, C., Carbonel, D., Guerrero, J., García-Hermoso, F., Zarroca, M., Linares, R., 2016. Sinkholes and caves related to evaporite dissolution in a stratigraphically and structurally complex setting, Fluvia Valley, eastern Spanish Pyrenees. Geological, geomorphological and environmental implications. Geomorphology 267, 76–97. https://doi.org/10.1016/j.geomorph.2016.05.018.

Gutiérrez, F., Fabregat, I., Roqué, C., Carbonel, D., Zarroca, M., Linares, R., Yechieli, Y., García-Arnay, Á., Sevil, J., 2019. Sinkholes in hypogene versus epigene karst systems, illustrated with the hypogene gypsum karst of the Sant Miquel de Campmajor Valley, NE Spain. Geomorphology 328, 57–78. https://doi.org/10.1016/j.geomorph.2018.12.003.

Jalali, L., Zarei, M., Gutiérrez, F., 2019. Salinization of reservoirs in regions with exposed evaporites. The unique case of Upper Gotvand Dam, Iran. Water Res. 157, 587–599. https://doi.org/10.1016/j.watres.2019.04.015.

Kaçaroğlu, F., Değirmenci, M., Cerit, O., 1997. Karstification in Miocene gypsum: an example from Sivas, Turkey. Environ. Geol. 30 (1), 88–97. https://doi.org/10.1007/s002540050136.

Kempe, S., 1996. Gypsum karst of Germany. Int. J. Speleol. 25 (3), 209–224. https://doi.org/10.5038/1827-806X.25.3.16.

Kergaravat, C., Ribes, C., Legeay, E., Callot, J.-P., Kavak, K.S., Ringenbach, J.-C., 2016. Minibasins and salt canopy in foreland fold-and-thrust belts: the central Sivas Basin, Turkey. Tectonics 35 (6), 1342–1366. https://doi.org/10.1002/2016TC004186.

Kergaravat, C., Ribes, C., Callot, J.-P., Ringenbach, J.-C., 2017. Tectono-stratigraphic evolution of salt-controlled minibasins in a fold and thrust belt, the Oligo-Miocene central Sivas Basin. J. Struct. Geol. 102, 75–97. https://doi.org/10.1016/j.jsg.2017.07.007.

Klimchouk, A.B., 2013. Evolution of intrastratal karst and caves in gypsum. In: Shroder, J.F. (Ed.), Treatise on Geomorphology. Academic Press, San Diego, pp. 438–450 https://doi.org/10.1016/B978-0-12-374739-6.00123-8.

Klimchouk, A., Cucchi, F., Calaforra, J.M., Aksem, S., Finocchiaro, F., Forti, P., 1996a. Dissolution of gypsum from field observations. Int. J. Speleol. 25 (3), 37–48. https://doi.org/10.5038/1827-806X.25.3.3.

Klimchouk, A., Forti, P., Cooper, A., 1996b. Gypsum karst of the world: a brief overview. Int. J. Speleol. 25 (3), 159–181. https://doi.org/10.5038/1827-806X.25.3.12.

Kurtman, F., 1973. Geologic and tectonic structure of the Sivas-Hafik-Zara and İmranlı Region. Maden Tetkik ve Arama Dergisi 80 (80), 1–38.

Legeay, E., Pichat, A., Kergaravat, C., Ribes, C., Callot, J.P., Ringenbach, J.C., Bonnel, C., Hoareau, G., Poisson, A., Mohn, G., Crumeyrolle, P., Kavak, K.S., Temiz, H., 2019. Geology of the Central Sivas Basin (Turkey). J. Maps 15 (2), 406–417. https://doi.org/10.1080/17445647.2018.1514539.

MTA, 2002. 1:500,000 Scale Geological Maps of Turkey.

Onal, K.M., Buyuksarac, A., Aydemir, A., Ates, A., 2008. Investigation of the deep structure of the Sivas Basin (innereast Anatolia, Turkey) with geophysical methods. Tectonophysics 460 (1), 186–197. https://doi.org/10.1016/j.tecto.2008.08.006.

Özel, S., Darıcı, N., 2020. Environmental hazard analysis of a gypsum karst depression area with geophysical methods: a case study in Sivas (Turkey). Environ. Earth Sci. 79 (5), 115. https://doi.org/10.1007/s12665-020-8861-4.

Parenti, C., Gutiérrez, F., Baioni, D., García-Arnay, Á., Sevil, J., Erica, L., 2020. Closed depressions in Kotido crater, Arabia Terra, Mars. Possible evidence of evaporite dissolution-induced subsidence. Icarus 341, 113680. https://doi.org/10.1016/j.icarus.2020.113680.

Paukštys, B., Cooper, A.H., Arustiene, J., 1999. Planning for gypsum geohazards in Lithuania and England. Eng. Geol. 52 (1), 93–103. https://doi.org/10.1016/S0013-7952(98)00061-1.

Pichat, A., Hoareau, G., Callot, J.-P., Legeay, E., Kavak, K.S., Révillon, S., Parat, C., Ringenbach, J.-C., 2018. Evidence of multiple evaporite recycling processes in a salt-tectonic context, Sivas Basin, Turkey. Terra Nova 30 (1), 40–49. https://doi.org/10.1111/ter.12306.

Poisson, A., Temiz, H., Gürsoy, H., 1992. Pliocene thrust tectonics in the Sivas basin near Hafik (Turkey): southward fore thrusts and associate northward backthrusts. Bull. Fac. Engin., Cumhuriyet Univ., Serie A–Earth Sci. 9, 19–25.

Poisson, A., Guezou, J.C., Ozturk, A., Inan, S., Temiz, H., Gürsöy, H., Kavak, K.S., Özden, S., 1996. Tectonic setting and evolution of the Sivas Basin, Central Anatolia, Turkey. Int. Geol. Rev. 38 (9), 838–853. https://doi.org/10.1080/00206819709465366.

Poisson, A., Vrielynck, B., Wernli, R., Negri, A., Bassetti, M.-A., Büyükmeriç, Y., Özer, S., Guillou, H., Kavak, K.S., Temiz, H., Orszag-Sperber, F., 2016. Miocene transgression in the central and eastern parts of the Sivas Basin (Central Anatolia, Turkey) and the Cenozoic palaeogeographical evolution. Int. J. Earth Sci. 105 (1), 339–368. https://doi.org/10.1007/s00531-015-1248-1.

Poyraz, M., Öztürk, M.Z., Soykan, A., 2021. Sivas jips karstında dolin yoğunluğunun CBS tabanlı analizi. Jeomorfolojik Araştırmalar Dergisi 6, 67–80. https://doi.org/10.46453/jader.863090.

Ribes, C., Kergaravat, C., Bonnel, C., Crumeyrolle, P., Callot, J.-P., Poisson, A., Temiz, H., Ringenbach, J.-C., 2015. Fluvial sedimentation in a salt-controlled mini-basin: stratal patterns and facies assemblages, Sivas Basin, Turkey. Sedimentology 62 (6), 1513–1545. https://doi.org/10.1111/sed.12195.

Ribes, C., Lopez, M., Kergaravat, C., Crumeyrolle, P., Poisson, A., Callot, J.-P., Paquette, J.-L., Ringenbach, J.-C., 2018. Facies partitioning and stratal pattern in salt-controlled marine to continental mini-basins: examples from the Late Oligocene to Early Miocene of the Sivas Basin, Turkey. Mar. Pet. Geol. 93, 468–496. https://doi.org/10.1016/j.marpetgeo.2018.03.018.

Shaw, M.G., Stafford, K.W., Tate, B.P., 2011. Surface denudation of the Gypsum Plain, West Texas and Southeastern New Mexico. In: Kuniansky, E.L. (Ed.), U.S. Geological Survey Karst Interest Group Proceedings, Fayetteville, Arkansas, April 26–29, 2011, U.S. Geological Survey Scientific Investigations Report 2011-5031, pp. 104–112.

Stafford, K.W., Nance, R., Rosales-Lagarde, L., Boston, P.J., 2008. Epigene and hypogene gypsum karst manifestations of the Castile Formation: Eddy County, New Mexico and Culberson County, Texas, USA. Int. J. Speleol. 37 (2), 83–98. https://doi.org/10.5038/1827-806X.37.2.1.

Taheri, K., Gutiérrez, F., Mohseni, H., Raeisi, E., Taheri, M., 2015. Sinkhole susceptibility mapping using the analytical hierarchy process (AHP) and magnitude–frequency relationships: a case study in Hamadan province, Iran. Geomorphology 234, 64–79. https://doi.org/10.1016/j.geomorph.2015.01.005.

Temiz, H., 1996. Tectonostratigraphy and thrust tectonics of the Central and Eastern parts of the Sivas Tertiary Basin, Turkey. Int. Geol. Rev. 38 (10), 957–971. https://doi.org/10.1080/00206819709465374.

Waltham, T., 2002. Gypsum karst near Sivas, Turkey. Cave Karst Sci. 29 (1), 39–44.

Waltham, T., 2004. Mulu, Sarawak. In: Gunn, J. (Ed.), Encyclopedia of Caves and Karst Science. Fitzroy Dearborn, New York, pp. 1134–1140.

Waltham, T., 2008. Sinkhole hazard case histories in karst terrains. Q. J. Eng. Geol. Hydrogeol. 41 (3), 291–300. https://doi.org/10.1144/1470-9236/07-211.

Waltham, T., Bell, F.G., Culshaw, M., 2005. Sinkholes and subsidence. Geophysical Sciences. Springer-Verlag, Berlin Heidelberg (384 pp).

Williams, P.W., 1972. Morphometric Analysis of Polygonal Karst in New Guinea. GSA Bull. 83 (3), 761–796. https://doi.org/10.1130/0016-7606(1972)83[761:MAOPKI]2.0.CO;2.

Williams, P.W., 2011. Karst in UNESCO World Heritage Sites. In: van Beynen, P.E. (Ed.), Karst Management. Springer Netherlands, Dordrecht, pp. 459–480 https://doi.org/10.1007/978-94-007-1207-2_21.

Yılmaz, I., 2007. GIS based susceptibility mapping of karst depression in gypsum: a case study from Sivas basin (Turkey). Eng. Geol. 90 (1), 89–103. https://doi.org/10.1016/j.enggeo.2006.12.004.

Yılmaz, I., 2012. On the value of dolines in gypsum terrains as a “Geological Heritage”: an example from Sivas basin, Turkey. Environ. Earth Sci. 65 (3), 805–812. https://doi.org/10.1007/s12665-011-1125-6.

Yılmaz, A., Yılmaz, H., 2006. Characteristic features and structural evolution of a post collisional basin: the Sivas Basin, Central Anatolia, Turkey. J. Asian Earth Sci. 27 (2), 164–176. https://doi.org/10.1016/j.jseaes.2005.02.006.

Yokoyama, R., Shirasawa, M., Pike, R., 2002. Visualizing topography by openness: a new application of image processing to digital elevation models. Photogramm. Eng. Remote Sens. 68 (3), 257–265.